

# Semantic Satellite Communications for Synchronized Audiovisual Reconstruction

Fangyu Liu, *Graduate Student Member, IEEE*, Peiwen Jiang, *Member, IEEE*,  
Wenjin Wang, *Member, IEEE*, Chao-Kai Wen, *Fellow, IEEE*, Xiao Li, *Member, IEEE*, and Shi Jin, *Fellow, IEEE*

**Abstract**—Satellite communications face severe bottlenecks in supporting high-fidelity synchronized audiovisual services, as conventional schemes struggle with cross-modal coherence under fluctuating channel conditions, limited bandwidth, and long propagation delays. To address these limitations, this paper proposes an adaptive multimodal semantic transmission system tailored for satellite scenarios, aiming for high-quality synchronized audiovisual reconstruction under bandwidth constraints. Unlike static schemes with fixed modal priorities, our framework features a dual-stream generative architecture that flexibly switches between video-driven audio generation and audio-driven video generation. This allows the system to dynamically decouple semantics, transmitting only the most important modality while employing cross-modal generation to recover the other. To balance reconstruction quality and transmission overhead, a dynamic keyframe update mechanism adaptively maintains the shared knowledge base according to wireless scenarios and user requirements. Furthermore, a large language model based decision module is introduced to enhance system adaptability. By integrating satellite-specific knowledge, this module jointly considers task requirements and channel factors such as weather-induced fading to proactively adjust transmission paths and generation workflows. Simulation results demonstrate that the proposed system significantly reduces bandwidth consumption while achieving high-fidelity audiovisual synchronization, improving transmission efficiency and robustness in challenging satellite scenarios.

**Index Terms**—Satellite communications, multimodal semantic communication, generative models, large language models, knowledge bases.

## I. INTRODUCTION

WITH the growing demand for global connectivity, satellite communications have become indispensable for maritime, aerial, and disaster-relief operations where terrestrial infrastructure is unavailable [1], [2]. However, links between ground stations and diverse user terminals are subject to severe physical layer constraints, including rain attenuation, significant Doppler shifts in non-geostationary orbits, and propagation delays exceeding several hundred milliseconds [3], [4]. Although conventional techniques such as adaptive modulation [5] and robust beamforming [6] can improve spectral efficiency, they struggle to support data-intensive multimodal streams, for example synchronized audiovisual

content, when transponder rates are limited to the kbps level. As a result, unpredictable satellite channel impairments remain a fundamental bottleneck for high-fidelity multimedia services.

Semantic communication has recently emerged as a promising paradigm to mitigate bandwidth limitations in satellite networks [7]. Unlike traditional communication systems, semantic communication improves transmission efficiency by extracting and transmitting only task-relevant semantics. Knowledge bases play a central role in this process by enabling context-aware transmission, enhancing inference capability, and substantially reducing data traffic [8], [9]. In satellite communications, a shared knowledge base between the transmitter and receiver enables adaptive semantic strategies, thereby maintaining transmission quality and efficiency under highly constrained channel conditions.

Prior studies have successfully applied semantic communication to text [10], [11] and images [12], [13]. However, video transmission remains a major bottleneck due to its massive data volume and the complexity of temporal sequences. Efficiently transmitting such bandwidth-intensive content is now a priority in the development of next-generation networks [14]–[17]. Existing semantic video transmission methods can be broadly classified into joint source-channel coding (JSCC) and generative model based approaches. As an early JSCC-based solution, DeepWiVe [14] jointly encodes and decodes multiple frames to exploit temporal correlations and improve transmission quality. Similarly, the DVST system [15] adopts nonlinear transformations and conditional encoding to extract inter-frame semantic features, achieving superior performance over conventional schemes. To further enhance efficiency, VISTA [16] separates video content into dynamic and static components for independent encoding. In contrast, generative model based approaches such as SVC [17] utilize pre-shared static frames as a knowledge base and transmit only key semantic features associated with content variations, from which the receiver generates the full video content, thereby substantially reducing transmission overhead with limited loss of visual fidelity.

Despite these advances, most existing methods focus on single modality video transmission, whereas practical applications often require synchronized audiovisual data, which demands higher content adaptability. Recent studies have explored cross-modal correlations for semantic encoding, including image-text transmission for visual question answering [18] and multimodal fusion for audiovisual event localization [19]. In video conferencing scenarios, several frameworks transmit 3D morphable model (3DMM) parameters to reconstruct facial

Fangyu Liu, Peiwen Jiang, Wenjin Wang, Xiao Li, and Shi Jin are with the School of Information Science and Engineering, Southeast University, Nanjing 210096, China (e-mail: fangyuliu@seu.edu.cn; peiwenjiang@seu.edu.cn; wangwj@seu.edu.cn; li\_xiao@seu.edu.cn; jinshi@seu.edu.cn).

Chao-Kai Wen is with the Institute of Communications Engineering, National Sun Yat-sen University, Kaohsiung 80424, Taiwan (e-mail: chaokai.wen@mail.nsysu.edu.tw).

videos and assist audio generation [20], or alternatively use text and audio to drive synchronized video synthesis [21]–[23]. However, modality prioritization and the selection of cross-modal generation paths in these methods are fixed at the design stage. This rigid configuration prevents the system from flexibly adjusting modality importance based on task requirements, such as prioritizing audio in emergency services. Moreover, existing knowledge base driven generative semantic systems [17], [20] generally lack context awareness and dynamic update mechanisms. This prevents the system from balancing generation performance with bandwidth consumption, leading to a dilemma of resource waste or outdated information in constrained channels. To address these limitations, the integration of generative foundation models, particularly large language models (LLMs) [24], offers a promising direction by enabling human-like contextual understanding and adaptive semantic allocation.

Besides content adaptability, the inherent instability of satellite links needs robust channel-adaptive transmission strategies. Strong inter-modality dependence makes multimodal systems vulnerable to cascading errors under channel fading. To address this, traditional approaches rely on rule-based or lookup-table methods. However, the complex interplay between satellite dynamics and diverse task requirements leads to an exponentially growing state space. This makes it impossible to enumerate all scenario combinations, often resulting in suboptimal strategy selection or improper resource allocation. To cope with such challenges, recent work has begun to exploit the reasoning and planning capabilities of LLMs to design active transmission strategies [25]. By dynamically sensing channel conditions and adjusting resource allocation, these approaches can mitigate the impact of fading. Incorporating foundation models into satellite semantic communication therefore enables adaptive optimization of both semantic compression and transmission reliability, ensuring stable end-to-end multimodal services under fluctuating channel conditions.

Motivated by the need for adaptability in uncertain environments, this paper proposes an adaptive semantic satellite transmission system governed by an LLM-based agent. Departing from traditional frameworks that passively execute fixed rules, this system marks a paradigm shift from static rule matching to intelligent planning. To enhance flexibility, a dual-stream multimodal generation module is employed, enabling dynamic switching between video-driven audio generation and audio-driven video generation. To balance reconstruction quality and bandwidth consumption, a dynamic keyframe update mechanism is introduced for knowledge base maintenance. Furthermore, serving as the core controller, the LLM-based agent coordinates these generation paths and update mechanisms. By understanding both task intent and physical constraints, the agent addresses key operational challenges that traditional methods cannot, ensuring high-fidelity synchronized reconstruction even in complex satellite scenarios. The main contributions of this work are summarized as follows.

- **Adaptive multimodal synchronization via dual-stream generative strategies:** The proposed system dynamically prioritizes key modality transmission by switching between video-driven and audio-driven generation accord-

ing to task requirements. This ensures high-fidelity audiovisual reconstruction and robust synchronization under severe satellite bandwidth constraints and channel fading.

- **Dynamic knowledge base management for bandwidth-quality trade-off:** A dynamic keyframe update mechanism is introduced to mitigate the impact of outdated shared knowledge bases. By adapting the update frequency to wireless conditions and user requirements, the system achieves an effective balance between reconstruction quality and bandwidth consumption in resource-constrained satellite environments.
- **Intelligent scenario- and task-aware adaptivity:** An LLM-based agent is integrated to optimize transmission efficiency and generation quality. Through real-time reasoning based on satellite conditions, user demands, and task characteristics, the agent dynamically adjusts semantic transmission paths and generation workflows, ensuring robustness across diverse satellite network scenarios.

The remainder of this paper is organized as follows. Section III describes the system model. Section IV presents the proposed framework. Section V provides experimental results. Finally, Section VI concludes the paper.

## II. RELATED WORK

In this section, we first examine the unique challenges of satellite communication and the limitations of end-to-end semantic paradigms. We then explore how generative artificial intelligence (AI) enhances semantic communication efficiency by leveraging prior knowledge, followed by an analysis of adaptation mechanisms for dynamic environments. Finally, key bottlenecks in current technologies are summarized to highlight the distinctions between the present work and prior research.

### A. Satellite Communication Systems

Satellite communication systems, particularly those based on low earth orbit (LEO) constellations, face physical layer challenges that are far more severe than those in traditional terrestrial cellular networks. A primary obstacle is the time-frequency fading caused by highly dynamic motion. With relative speeds of approximately 7.6 km/s, LEO satellites experience significant Doppler shifts. These shifts not only disturb the orthogonality between orthogonal frequency-division multiplexing (OFDM) subcarriers, leading to inter-carrier interference [26], but also result in very short channel coherence times. Consequently, the channel state information (CSI) obtained at the transmitter and receiver becomes outdated rapidly during transmission, severely degrading the accuracy of beamforming and link adaptation. Additionally, power constraints and long delays limit transmission efficiency. The significant free-space path loss (FSPL) [27] typically results in the downlink operating in low signal-to-noise ratio (SNR) regions. While hybrid automatic repeat request (HARQ) is commonly used to ensure reliability, the high delays introduced by the satellite links severely diminish throughput efficiency due to frequent handshakes and retransmissions [28]–[30].

Faced with these challenges, traditional communication technologies, which are approaching the Shannon limit, struggle to support high-bandwidth multimedia transmission. As a result, deep learning has been proposed as a key technology for addressing the complexities of satellite communication [31]. In particular, semantic communication offers a breakthrough by extracting task-relevant core features rather than transmitting all bits, providing a new approach for efficient transmission over constrained channels. Some early studies have begun to explore the application of semantic communication in non-terrestrial networks, such as in computation offloading [32] and image transmission [33].

### B. End-to-End Semantic Communication

To overcome the transmission challenges in poor channel conditions, JSCC has emerged as an end-to-end semantic communication paradigm. It aims to break the bottleneck of the traditional separation theorem by jointly optimizing source compression and channel coding. Recent efforts have sought to establish formal mathematical models for this paradigm. For instance, the semantic rate-distortion theory was proposed in [34], while semantic entropy was defined in [35] based on the source information. These works provide essential theoretical guidance and quantitative foundations for JSCC-based semantic communication.

With the introduction of deep learning, the end-to-end JSCC framework based on autoencoders can directly learn nonlinear mappings from high-dimensional source data to continuous channel symbols, effectively mitigating the cliff effect observed in traditional digital transmission. The Deep-JSCC framework [12] demonstrates that neural networks could map image pixels directly to complex channel symbols, significantly outperforming traditional JPEG and low-density parity-check (LDPC)-based schemes in terms of reconstruction quality under low SNR and limited bandwidth constraints. This paradigm was quickly extended to adaptive transmission [36], [37], multiple-input multiple-output (MIMO) systems [38], and video transmission using temporal correlations [14]–[16]. For text transmission, a deep semantic communication system based on Transformer architecture was proposed in [39]. This system implements JSCC to minimize semantic errors by maximizing semantic similarity, rather than the bit-level accuracy typical of traditional systems, thereby significantly enhancing capacity. This paradigm was further extended to speech [40], [41] and point cloud data [42].

However, despite the improvements in robustness, end-to-end semantic communication still faces limitations in semantic fidelity. Most existing JSCC models essentially rely on pixel- or waveform-level approximation, and at extremely low compression rates, they often produce blurry reconstructions, failing to recover high-frequency details using external knowledge. This limitation has shifted research focus toward more powerful AI models with stronger generative capabilities.

### C. Generative Model-Assisted Semantic Communication

The breakthrough advancements in generative AI, particularly generative adversarial networks [43], diffusion models

[44], and LLMs [45], have propelled semantic communication toward a generative paradigm. The core idea is to leverage powerful generative priors as shared knowledge bases, transmitting only minimal semantic information and reconstructing high-quality content at the receiver.

Compared to end-to-end JSCC, generative semantic communication offers greater flexibility and compression. It can tailor strategies to specific transmission tasks by only transmitting key semantic features required for the task, significantly reducing transmission overhead without compromising downstream task performance. For example, in video conferencing scenarios, facial detail restoration was achieved in [17], [20] by transmitting only facial keypoints or 3DMM parameters, combined with pre-shared static knowledge bases. Similarly, [46]–[48] proposed transmitting only the textual content of the speech [46] and using speech generative models [49] at the receiver to synthesize the speech, significantly reducing bandwidth requirements.

While these early methods often employed small-scale, task-specific extraction and generation networks, such networks lacked generalization capability for diverse real-world applications and increased system complexity. In contrast, foundation models possess strong representational and generalization learning capabilities, enabling them to effectively handle complex tasks and accurately understand the subtleties and implied meanings in language [50], [51]. To address the poor generalization of earlier specialized models, foundation models have been introduced into semantic communication. For instance, the segment anything model [52] was incorporated in [53] for image semantic transmission, utilizing its zero-shot generalization ability for efficient segmentation. Additionally, pre-trained LLMs (e.g., ChatGPT [24]) can more effectively evaluate the importance of transmitted content, using their strong contextual prediction ability to correct and complete semantics [54], thereby improving transmission robustness. Furthermore, foundation models are widely used in text- or other condition-guided image generation [55]–[57] to achieve high-fidelity semantic transmission under low bandwidth.

Despite excelling in source compression and generation, generative semantic communication often overlooks physical layer robustness. Most existing generative transceivers treat the channel as a black box or assume a static Gaussian channel, failing to utilize channel environment information to assist semantic encoding and decoding. In dynamic environments like LEO satellite communications, characterized by Doppler shifts and long delays, ignoring the physical layer characteristics in design can lead to semantic errors or even completely erroneous content generation.

### D. Semantic Transmission Adaptation for Dynamic Environments

To ensure the reliability of semantic transmission in dynamic channels, system design must evolve toward environmental awareness and adaptation. This requires physical layers to dynamically allocate resources based on semantic importance and real-time channel conditions for differentiated protection.

TABLE I  
COMPARISON OF THE PROPOSED SYSTEM WITH EXISTING SEMANTIC TRANSMISSION SCHEMES

Reference	Core Mechanism	Channel Adaptation	Cross-Modal Synthesis	Modality Priority	Dynamic KB	Active Planning
<i>Video Semantic Transmission Methods</i>						
[14]	JSCC based on multiple frame temporal correlation	✓(Passive)	×	×	×	×
[15]	JSCC based on nonlinear transformation encoding	✓(Passive)	×	×	×	×
[16]	JSCC based on content aware coding	✓(Passive)	×	×	×	×
[17]	Video generation based on key points	✓(Passive)	×	×	×	×
<i>Audio Semantic Transmission Methods</i>						
[40]	End to end speech waveform encoding and decoding	×	×	×	×	×
[47], [48]	Speech synthesis based on transmitted text	×	×	×	×	×
[41]	SNR based adaptive coding	✓(Passive)	×	×	×	×
<i>Multimodal Synchronous Semantic Transmission Methods</i>						
[20]	Video-driven cross-modal audio generation	✓(Passive)	✓	×	×	×
[21]–[23]	Audio-driven cross-modal video generation	✓(Passive)	✓	×	×	×
<b>Ours</b>	<b>LLM-guided adaptive dual-stream generation</b>	<b>✓(Proactive)</b>	<b>✓</b>	<b>✓</b>	<b>✓</b>	<b>✓</b>

Note: ✓ denotes supported feature; × denotes unsupported. “Passive” indicates implicit adaptation via training, while “Proactive” indicates agent-based planning.

Early research primarily focused on static resource allocation based on importance. For example, [58]–[60] allocated channels and designed MIMO precoding to prioritize transmitting high-entropy or key semantic features over high-quality subchannels. Deep learning was further utilized in [61] to evaluate the semantic importance of content and prioritize key content through power allocation, improving overall recovery performance under poor channel conditions. To counteract channel fluctuations, an enhanced HARQ technique was introduced in [62] at the physical layer, intelligently deciding whether to retransmit corrupted semantic features. Moreover, an SNR-adaptive speech semantic transmission system was proposed in [63]. This system maps speech signals to a semantic latent space via nonlinear transformations and establishes an entropy model within that space based on variational modeling to evaluate the importance of semantic features. By incorporating channel SNR as tokens in the network architecture, the system achieved high coding gain and adapted to various channel conditions, thereby improving robustness. Additionally, reinforcement learning was leveraged in [64] to adaptively allocate transmission resources based on semantic value, yielding superior semantic fidelity and higher user satisfaction.

However, these methods mainly focus on passive adaptation to channel conditions and lack the ability to autonomously perceive environmental changes and formulate proactive strategies. In extremely dynamic and unknown environments, such as high-speed trains or LEO satellite communications, significant Doppler shifts and large delays cause CSI feedback to become outdated. Resource allocation based on outdated information can lead to resource mismatch and performance degradation. Furthermore, existing systems lack a cognitive agent capable of deeply understanding the nonlinear coupling between the channel, semantics, and tasks. Without the ability

to comprehend the evolution of complex channel environments and make forward-looking cross-layer decisions to diverse task requirements, robustness remains insufficient in dynamic scenarios.

### E. Summary and Key Challenges

In summary, semantic communication has shifted from end-to-end optimized coding to generative model-based semantic reconstruction. While both approaches have made significant progress in transmission robustness and content compression efficiency, they still reveals several critical limitations when applied to satellite audiovisual synchronization scenarios. Based on the review above, the key challenges and lessons learned are summarized as follows:

- **Disconnection between semantic and physical layer design:** Most semantic transmission systems simplify the wireless channel into a black box, overlooking its dynamic fading characteristics. Conversely, physical layer adaptation schemes, as discussed in Section II-D, typically optimize bit-level metrics without awareness of multimodal semantic importance. In resource-limited satellite environments, this cross-layer isolation prevents the system from prioritizing critical semantic features, leading to task failure when key information is lost during deep fading.
- **Rigid cross-modal dependencies:** Existing architectures lack flexibility in handling diverse task requirements. Many methods rely on fixed, unidirectional generation logic (e.g., solely generating video from audio). This rigidity is ill-suited for satellite service scenarios where priorities shift dynamically. For instance, surveillance tasks demand high video fidelity, whereas voice scheduling requires prioritized audio intelligibility. The inability

to decouple or reconfigure these dependencies limits system versatility.

- **Ineffectiveness of passive channel adaptation:** Traditional feedback-based mechanisms (e.g., HARQ) suffer from severe information outdateding in satellite communication due to long propagation delays. These passive approaches lack a cognitive agent capable of predicting channel evolution. Consequently, resource allocation decisions consistently lag behind the rapid channel variations of non-terrestrial networks, resulting in significant performance degradation.

To overcome these limitations, this work proposes an LLM-driven multimodal semantic communication system. The system achieves flexible cross-modal dependency configuration through a dual-stream generation architecture and utilizes an intelligent agent to implement forward-looking, joint semantic-physical layer decisions. A detailed comparison between the proposed scheme and existing works is presented in Table I.

### III. SYSTEM MODEL

In this section, we first describe the semantic satellite communication environment, followed by an overview of the multimodal semantic transmission framework.

#### A. Semantic Satellite Communication Scenarios

This paper considers a satellite-based multimodal transmission scenario, transmitting face videos and corresponding audio, as shown in Fig. 1. The ground transmitter performs task-oriented semantic encoding on the audio and video data and transmits them to the satellite. The satellite, acting as a relay, forwards the received semantic features through the downlink to the ground receiver for reconstruction. The design of such a system is primarily challenged by the following factors.

- **Dynamic and constrained channel:** The satellite link is affected by FSPL, rainfall attenuation (RA) [65], and Doppler shifts caused by high-speed motion. To ensure reliable transmission, conservative modulation and coding schemes are required, which severely limit the effective bandwidth and throughput.
- **Diverse service requirements:** Satellite services support heterogeneous applications. For example, video conferencing prioritizes audiovisual synchronization, whereas disaster broadcasting emphasizes audio intelligibility. Such diversity necessitates a task-aware adaptive transmission strategy under limited resources.

#### B. Semantic Transmission Framework

To transmit multimodal audiovisual data  $\mathbf{M}$ ,  $\mathbf{M}$  is first decomposed into video  $\mathbf{V}$  and the corresponding audio  $\mathbf{A}$ . At the ground transmitter, semantic source encoding is applied to extract essential features, given by

$$\mathbf{S}_{\text{video}} = S_{\text{video}}(\mathbf{V}), \quad (1)$$

$$\mathbf{S}_{\text{audio}} = S_{\text{audio}}(\mathbf{A}), \quad (2)$$

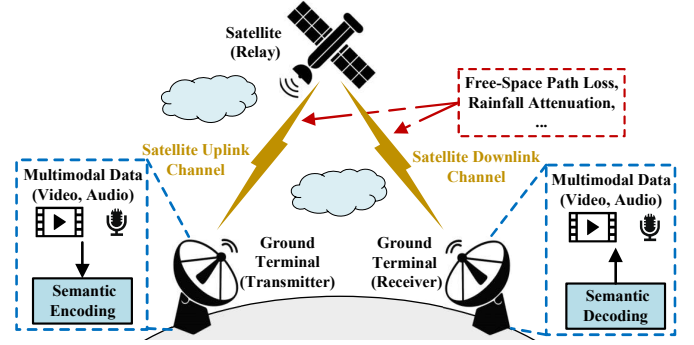


Fig. 1. System model of satellite-ground transmission, including satellite, transmission link, and ground terminal.

where  $\mathbf{S}_{\text{video}}$  and  $\mathbf{S}_{\text{audio}}$  denote the extracted semantic features, and  $S_{\text{video}}(\cdot)$  and  $S_{\text{audio}}(\cdot)$  represent the semantic source encoders. To preserve audiovisual synchronization,  $\mathbf{S}_{\text{video}}$  and  $\mathbf{S}_{\text{audio}}$  are multiplexed into a unified data stream and mapped onto OFDM symbols  $\mathbf{X}$  with  $N_t$  time symbols and  $N_f$  subcarriers.

After transmission over the uplink and downlink channels, the received signal at the ground terminal is expressed as

$$\mathbf{Y} = \mathbf{H}_{\text{down}} \odot \mathbf{H}_{\text{up}} \odot \mathbf{X} + \mathbf{Z}, \quad (3)$$

where  $\odot$  denotes element-wise multiplication,  $\mathbf{Z}$  represents additive noise, and  $\mathbf{H}_{\text{up}} \in \mathbb{C}^{N_f \times N_t}$  and  $\mathbf{H}_{\text{down}} \in \mathbb{C}^{N_f \times N_t}$  are the uplink and downlink channel frequency responses, respectively. The corresponding channel impulse response is modeled as

$$h(t, \tau) = \sum_{l=0}^{L-1} h_l \delta(\tau - \tau_l) \exp(j2\pi f_l t), \quad (4)$$

where  $L$  is the number of channel taps,  $h_l$  denotes the channel gain,  $\tau_l$  is the propagation delay, and  $f_l$  is the Doppler shift of the  $l$ th path.

Small-scale fading effects, such as Doppler shifts, can be mitigated by OFDM and dense pilot-aided channel estimation. However, large-scale fading caused by long propagation distance and weather conditions, including FSPL and RA, significantly degrades the received SNR. The FSPL [27] is given by

$$\text{FSPL}(\text{dB}) = 20 \log_{10}(d) + 20 \log_{10}(f) - 147.56, \quad (5)$$

where  $f$  is the carrier frequency in hertz, and  $d$  is the satellite link distance in meters, determined by the orbit altitude and the ground terminal elevation angle. RA refers to signal degradation caused by propagation through rain regions. According to the ITU R P.618 model [65], the attenuation is expressed as

$$\text{RA}(\text{dB}) = \gamma_R \cdot L_e, \quad (6)$$

where  $\gamma_R$  is the specific attenuation determined by rainfall rate and carrier frequency, and  $L_e$  is the effective path length through the rain region.

Accordingly, the SNR of the satellite link [66] is given by

$$\text{SNR}(\text{dB}) = P_t + G_t + G_s + G_r - \text{RA}_{\text{all}} - \text{FSPL}_{\text{all}} - N, \quad (7)$$

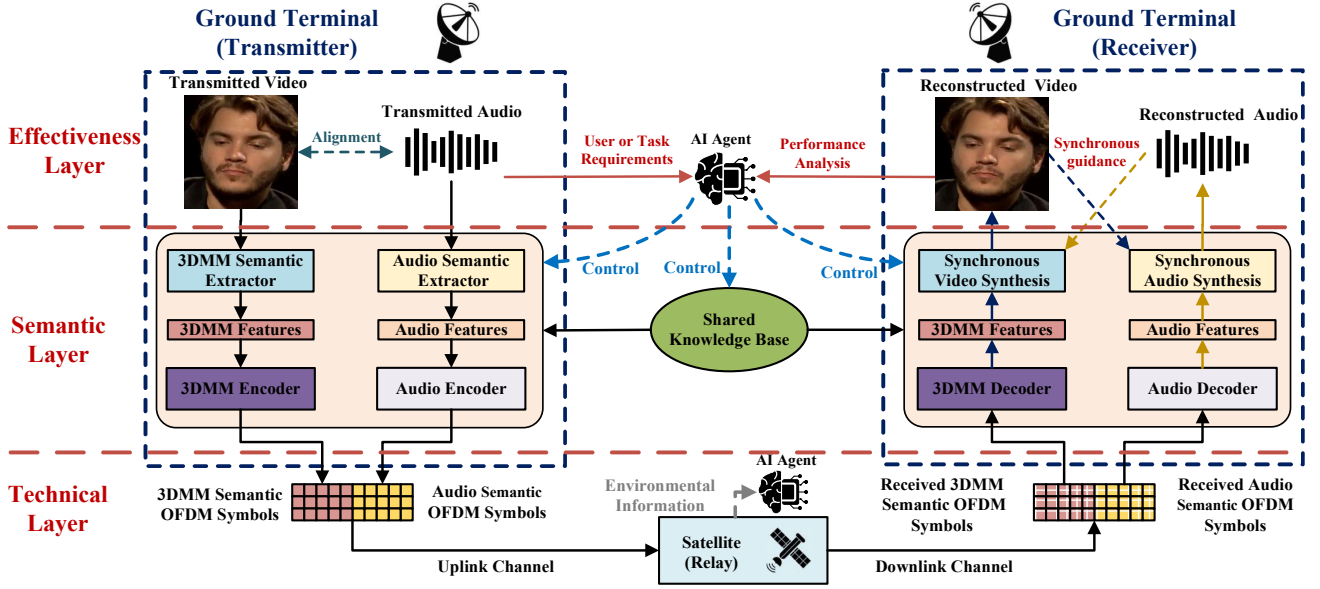


Fig. 2. Structure of the proposed adaptive audiovisual synchronous semantic transmission system for satellite communication scenarios.

where  $P_t$  is the transmit power in dBm,  $G_t$  and  $G_r$  are the transmit and receive antenna gains in dBi,  $G_s$  is the equivalent gain of the relay satellite,  $FSPL_{all}$  and  $RA_{all}$  are the total FSPL and RA of the satellite channel, respectively, and  $N$  denotes the receiver thermal noise power, computed as  $N = 10 \log_{10}(kTB)$ . Here,  $k$  is the Boltzmann constant,  $B$  is the system bandwidth, and  $T$  is the noise temperature.

At the receiver, an estimate  $\hat{H}$  is obtained via least-squares channel estimation, and equalization yields

$$\hat{\mathbf{X}} = \mathbf{Y} \oslash \hat{\mathbf{H}}, \quad (8)$$

where  $\oslash$  denotes element-wise division. The noisy semantic features  $\hat{\mathbf{S}}_{video}$  and  $\hat{\mathbf{S}}_{audio}$  are extracted from  $\hat{\mathbf{X}}$  and fed into the semantic decoder for synchronized audiovisual reconstruction, given by

$$\hat{\mathbf{V}}, \hat{\mathbf{A}} = S_{sync}(\hat{\mathbf{S}}_{video}, \hat{\mathbf{S}}_{audio}, \mathbf{KB}), \quad (9)$$

where  $S_{sync}(\cdot)$  denotes the synchronization-aware semantic decoder. Depending on task requirements, it adaptively selects either video-driven audio generation or audio-driven video generation. The semantic knowledge base  $\mathbf{KB}$ , similar to [17], [20], contains the user reference image and supports identity-consistent video generation.

#### IV. PROPOSED ADAPTIVE AUDIOVISUAL SYNCHRONOUS SEMANTIC TRANSMISSION SYSTEM

In this section, we first present the proposed system framework and describe the dual-stream audiovisual semantic coding process. We then analyze the impact of shared keyframes on generative performance, followed by a dynamic knowledge base updating mechanism designed for diverse application scenarios. Finally, an LLM-based decision module is introduced to adaptively optimize transmission paths and generation workflows under varying satellite channel conditions.

##### A. System Framework

As shown in Fig. 2, the proposed system consists of three core layers, namely the effectiveness layer, the semantic layer, and the technical layer, all integrated with a shared semantic knowledge base. These components jointly optimize transmission performance for resource-constrained satellite links.

1) *Effectiveness Layer*: The effectiveness layer focuses on semantic transmission quality and user experience by evaluating task-specific performance metrics, such as facial video reconstruction fidelity and audio semantic accuracy.

2) *Semantic Layer*: Guided by the LLM agent, the semantic transmitter selectively extracts task-relevant features from video  $\mathbf{V}$  and audio  $\mathbf{A}$ . Unlike single-modal SVC [17] or fixed-priority schemes [20]–[23], our design enables flexible semantic decoupling. By leveraging cross-modal generative capabilities, the system can dynamically omit less important modalities when bandwidth is limited, relying on the remaining modality to generate the missing content. At the receiver, reconstruction follows one of two adaptive workflows.

- **Video-driven audio generation (V2A)**: Designed for scenarios prioritizing visual fidelity, where text and 3DMM parameters are transmitted. The system first reconstructs the video content. The reconstructed video then guides the network to synthesize synchronized audio from the text, ensuring audiovisual synchronization.
- **Audio-driven video generation (A2V)**: Designed for scenarios prioritizing audio accuracy, this system transmits only the audio semantics, including text and acoustic features such as duration, and first reconstructs the audio. The video generation network then synthesizes synchronized video based on the reconstructed audio.

3) *Technical Layer*: The technical layer manages the physical transmission of semantic features over the satellite channel. In addition, it provides real-time environmental information, such as satellite identification, user location, and weather

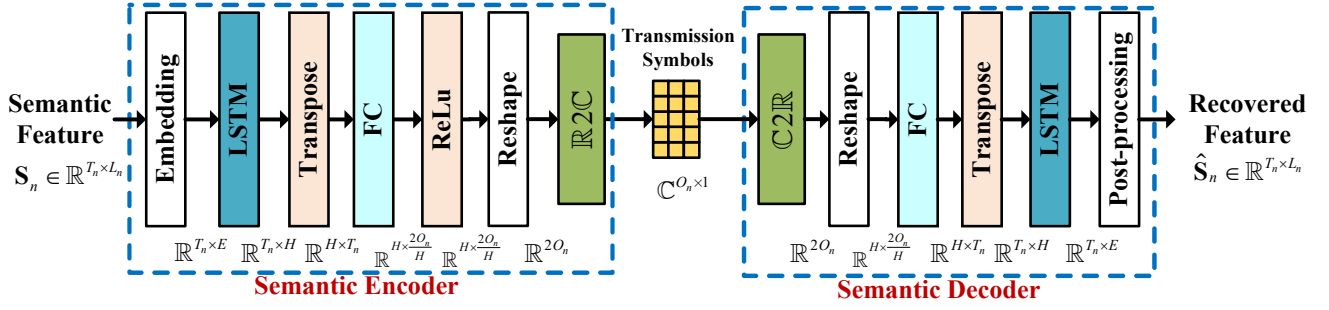


Fig. 3. Architecture of the temporal semantic encoder and decoder.

conditions, to the LLM agent, enabling dynamic optimization of transmission strategies and network parameters.

4) *Semantic Knowledge Base*: The semantic knowledge base consists of explicit and implicit components. The explicit knowledge base stores relatively static information, such as user appearance, that is shared between the transmitter and receiver. Updates are required in scenarios involving user changes or significant pose variations. Due to satellite bandwidth constraints, these updates are strategically scheduled during periods of stable channel conditions. The implicit knowledge base is embedded within the semantic encoder and decoder through end-to-end training. It requires fine-tuning or retraining to adapt to evolving system scenarios. The design and implementation details of each module are presented in the following sections.

### B. Semantic Feature Extraction and Encoding/Decoding

Facial dynamics in audiovisual content are mainly characterized by posture, expressions, and lip movements. Thus, a subset of 3DMM parameters [67] is adopted as the key video semantics, which significantly reduces data volume and is well-suited for bandwidth-constrained satellite links. At the receiver, these parameters, together with keyframes from the shared knowledge base, guide the generation of dynamic facial video.

Let  $\mathbf{V} \in \mathbb{R}^{T_V \times 256 \times 256 \times 3}$  denote a video clip of length  $T_V$ , where the first frame  $\mathbf{V}_1$  captures the user appearance. When the update condition is satisfied, this frame is used to update the knowledge base at both the transmitter and receiver. The subsequent frames are then processed by the 3DMM semantic extractor. The extraction process for the  $i$ th frame is given by

$$\mathbf{s}_i = f_{3\text{DMM}}(\mathbf{V}_i; \Theta_{3\text{DMM}}), \quad (10)$$

where  $f_{3\text{DMM}}(\cdot)$  is the pre-trained 3DMM extraction model [68] with fixed parameters  $\Theta_{3\text{DMM}}$ . The vector  $\mathbf{s}_i = [\mathbf{s}_{i,\text{id}}, \mathbf{s}_{i,\text{exp}}, \mathbf{s}_{i,\text{rot}}, \mathbf{s}_{i,\text{trans}}]$  comprises identity, expression, rotation, and translation coefficients. Since identity information is retained in the shared knowledge base,  $\mathbf{s}_{i,\text{id}}$  is excluded from transmission. Furthermore, as the first six dimensions of  $\mathbf{s}_{i,\text{exp}}$  capture most of the expression variations, only these coefficients are transmitted. Therefore, the transmitted semantic set for the  $i$ th frame is denoted as

$$\mathbf{S}_{i,\text{M}} = \{\mathbf{s}_{i,\text{exp}}[1:6], \mathbf{s}_{i,\text{rot}}, \mathbf{s}_{i,\text{trans}}\}, \quad (11)$$

while the aggregated semantics for the entire video are denoted as  $\mathbf{S}_M$ .

For the audio signal  $\mathbf{A}$  aligned with the video, we extract deep semantic features, including text, phonemes, and duration. Text conveys linguistic content, while phonemes and duration capture the acoustic characteristics of the audio. The extraction process is formulated as

$$\mathbf{S}_T, \mathbf{S}_P, \mathbf{S}_D = f_{\text{audio}}(\mathbf{A}; \Theta_{\text{audio}}), \quad (12)$$

where  $\mathbf{S}_T$ ,  $\mathbf{S}_P$ , and  $\mathbf{S}_D$  denote the extracted text, phonemes, and duration, respectively. The function  $f_{\text{audio}}(\cdot)$  employs Whisper-small [69] for automatic speech recognition and the Montreal Forced Aligner [70] for acoustic feature extraction.

Since  $\mathbf{S}_M$ ,  $\mathbf{S}_T$ ,  $\mathbf{S}_P$ , and  $\mathbf{S}_D$  are time-dependent sequences, a temporal encoder-decoder architecture, as illustrated in Fig. 3, is adopted to mitigate the impact of satellite channel fading. The encoding process is given by

$$\mathbf{X}_n = f_{\text{en},n}(\mathbf{S}_n; \Theta_{\text{en},n}), \quad n \in \{\text{M}, \text{T}, \text{P}, \text{D}\}, \quad (13)$$

where  $\mathbf{X}_n$  is the encoded symbol, while  $f_{\text{en},n}(\cdot)$  and  $\Theta_{\text{en},n}$  represent the corresponding semantic feature encoder and its parameters, respectively. At the receiver, features are reconstructed through the corresponding semantic decoders as

$$\hat{\mathbf{S}}_n = f_{\text{de},n}(\hat{\mathbf{X}}_n; \Theta_{\text{de},n}), \quad n \in \{\text{M}, \text{T}, \text{P}, \text{D}\}, \quad (14)$$

where  $\hat{\mathbf{S}}_n$  denotes the recovered semantic features, and  $f_{\text{de},n}(\cdot)$  is the decoder operation with parameters  $\Theta_{\text{de},n}$ .

We distinguish between floating-point data ( $\mathbf{S}_M$ ,  $\mathbf{S}_D$ ) and token sequences ( $\mathbf{S}_T$ ,  $\mathbf{S}_P$ ), and apply distinct encoding and decoding strategies, as illustrated in Fig. 3. For floating-point inputs, the embedding layer employs linear projection to map  $\mathbb{R}^{T_n \times L_n}$  to  $\mathbb{R}^{T_n \times E}$ , where  $T_n$  is the temporal length,  $L_n$  is the input feature dimension, and  $E$  is the embedding dimension. For token sequences, a lookup table  $\Psi_n$  encodes tokens into embeddings, which are further projected to  $\mathbb{R}^{T_n \times E}$ . In the decoder, floating-point outputs are recovered using a single fully-connected layer, whereas token sequence outputs are obtained through a fully-connected layer followed by a softmax function and an argmax operation.

The training process for these encoder-decoder models is defined as

$$(\hat{\Theta}_{\text{en},n}, \hat{\Theta}_{\text{de},n}) = \underset{\Theta_{\text{en},n}, \Theta_{\text{de},n}}{\text{argmin}} \mathcal{L}_n(\mathbf{S}_n, f_{\text{de},n}(f_{\text{en},n}(\mathbf{S}_n; \Theta_{\text{en},n}); \Theta_{\text{de},n})), \quad (15)$$

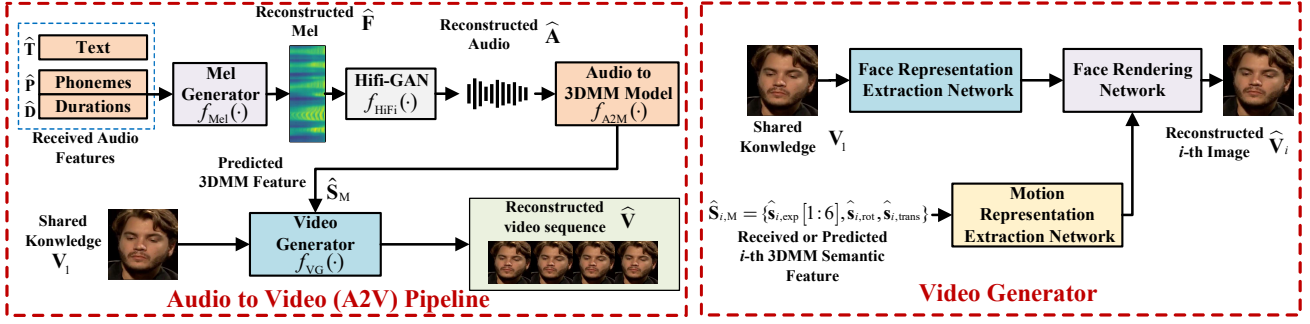


Fig. 4. Pipeline of the audio-driven video generation (A2V) and the structure of the video generator.

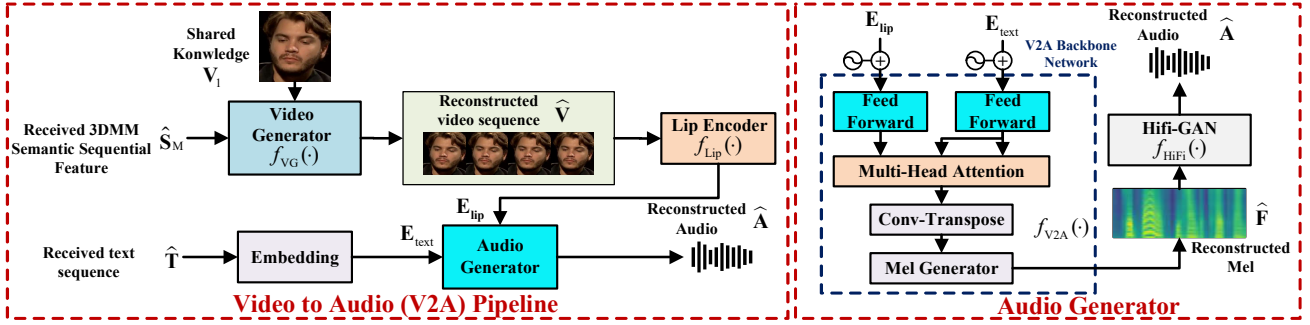


Fig. 5. Pipeline of the video-driven audio generation (V2A) and the structure of the audio generator.

where  $\mathcal{L}_n$  is the loss function. Specifically, mean-squared error (MSE) is employed for  $\mathbf{S}_M$  and  $\mathbf{S}_D$ , while cross-entropy loss is utilized for  $\mathbf{S}_T$  and  $\mathbf{S}_P$ .

### C. Multimodal Synchronous Generation Network

Due to limited satellite bandwidth, the system uses a task-dependent selective transmission strategy. Instead of transmitting full multimodal data, only the essential semantic features required for the task are transmitted. At the receiver, these semantics are used to reconstruct the primary modality and guide the generation of the omitted modality. These two workflows are detailed below.

1) *Audio-Driven Video Generation (A2V)*: This workflow is designed for scenarios prioritizing audio accuracy, while audio semantics such as text, phonemes, and duration are transmitted. The received semantics are first used to reconstruct the audio  $\hat{\mathbf{A}}$ , as illustrated in Fig. 4. The reconstructed phonemes  $\hat{\mathbf{S}}_P$  and duration  $\hat{\mathbf{S}}_D$  are processed by the Mel-spectrogram generator  $f_{\text{Mel}}(\cdot)$  [71], followed by the vocoder  $f_{\text{HiFi}}(\cdot)$  [72], to reconstruct the audio waveform, which can be expressed as

$$\hat{\mathbf{A}} = f_{\text{HiFi}} \left( f_{\text{Mel}} \left( \hat{\mathbf{S}}_P, \hat{\mathbf{S}}_D; \Theta_{\text{Mel}} \right); \Theta_{\text{HiFi}} \right), \quad (16)$$

where  $\Theta_{\text{Mel}}$  and  $\Theta_{\text{HiFi}}$  denote the parameters of  $f_{\text{Mel}}(\cdot)$  and  $f_{\text{HiFi}}(\cdot)$ , respectively.

Subsequently,  $\hat{\mathbf{A}}$  is fed into the pre-trained audio-to-3DMM module  $f_{\text{A2M}}(\cdot)$  [73] to predict the 3DMM coefficients  $\hat{\mathbf{S}}_M$ , which is formulated as

$$\hat{\mathbf{S}}_M = f_{\text{A2M}} \left( \hat{\mathbf{A}}; \Theta_{\text{A2M}} \right), \quad (17)$$

where  $\Theta_{\text{A2M}}$  denotes the parameters of  $f_{\text{A2M}}(\cdot)$ . This module first maps the audio signal into an audio feature representation

and then predicts the corresponding 3DMM coefficients. As the module is trained on a large-scale audio-3DMM paired dataset, it effectively learns the mapping from audio to facial deformation.

Finally, the video generator  $f_{\text{VG}}(\cdot)$  [73] synthesizes consecutive video frames, as illustrated in Fig. 4. For the  $i$ th frame with coefficients  $\hat{\mathbf{S}}_{i,M}$ , the generation process is defined as

$$\hat{\mathbf{V}}_i = f_{\text{VG}} \left( \hat{\mathbf{S}}_{i,M}, \mathbf{V}_1; \Theta_{\text{VG}} \right), \quad (18)$$

where  $\mathbf{V}_1$  is the reference image that provides identity information from the knowledge base. Specifically, the motion representation extraction network converts the facial deformation and pose information in  $\hat{\mathbf{S}}_{i,M}$  into motion control features. These features, together with the static appearance features provided by  $\mathbf{V}_1$ , are then fed into the rendering network to animate the reference image, thereby generating the  $i$ th video frame  $\hat{\mathbf{V}}_i$ .

2) *Video-Driven Audio Generation (V2A)*: This workflow is designed for scenarios prioritizing visual fidelity, where text and 3DMM parameters are transmitted. As illustrated in Fig. 5, the received 3DMM parameters  $\hat{\mathbf{S}}_M$  and the shared reference image  $\mathbf{V}_1$  are fed into the video generator  $f_{\text{VG}}(\cdot)$  to synthesize the video sequence according to (18).

Audiovisual synchronization is reflected in the coordination between lip movements and audio content. Therefore, the generated video  $\hat{\mathbf{V}}$  is used to guide the generation of time-aligned audio. Specifically, the lip region of the generated video is processed by a lip encoder  $f_{\text{Lip}}(\cdot)$  [74] to extract lip motion features, which can be expressed as

$$\mathbf{E}_{\text{lip}} = f_{\text{Lip}}(\hat{\mathbf{V}}) \in \mathbb{R}^{T_V \times D_m}, \quad (19)$$

where  $D_m = 256$  is the dimension of the lip features.

The received text is converted into embedding vectors  $\mathbf{E}_{\text{text}} \in \mathbb{R}^{1 \times D_m}$ . A multi-head attention mechanism is then employed to learn the correlation between lip shapes and text embeddings [75], guiding the audio generation process, which is formulated as

$$\begin{aligned} \mathbf{E}_{\text{lip-text}} &= \text{Attention}(\mathbf{E}_{\text{lip}}, \mathbf{E}_{\text{text}}, \mathbf{E}_{\text{text}}) \\ &= \text{Softmax} \left( \frac{\mathbf{E}_{\text{lip}} \mathbf{E}_{\text{text}}^\top}{\sqrt{D_m}} \right) \mathbf{E}_{\text{text}}, \end{aligned} \quad (20)$$

where  $\mathbf{E}_{\text{lip-text}} \in \mathbb{R}^{T_V \times D_m}$  is the aligned lip-text features,  $\top$  is the transpose operation. According to [75], in synchronized audiovisual clips, the Mel-spectrogram length  $T_{\text{Mel}}$  is required to be  $f_{\text{expan}}$  times that of the video frames  $T_V$ . Therefore,  $\mathbf{E}_{\text{lip-text}}$  is expanded by a factor of  $f_{\text{expan}}$  using transposed convolution. The expansion factor  $f_{\text{expan}}$  is defined as

$$f_{\text{expan}} = \frac{T_{\text{Mel}}}{T_V} = \frac{sr/hs}{FPS} \in \mathbb{N}^+, \quad (21)$$

where  $sr$ ,  $hs$ , and  $FPS$  denote the audio sampling rate, the hop size used for Mel-spectrogram calculation, and the video frame rate, respectively.

The aligned features  $\mathbf{E}_{\text{lip-text}}$  are then converted into a Mel-spectrogram sequence  $\hat{\mathbf{F}}$  by the generator  $f_{\text{Mel}}(\cdot)$ , and the audio waveform is synthesized by the vocoder  $f_{\text{HiFi}}(\cdot)$ . The synthesis process is expressed as

$$\hat{\mathbf{A}} = f_{\text{HiFi}}(\hat{\mathbf{F}}; \Theta_{\text{HiFi}}) = f_{\text{HiFi}}(f_{\text{Mel}}(\mathbf{E}_{\text{lip-text}}; \Theta_{\text{Mel}}); \Theta_{\text{HiFi}}). \quad (22)$$

Let  $f_{\text{V2A}}(\cdot)$  denote the V2A backbone network, which consists of the attention module, transposed convolution, and Mel-spectrogram generator, with parameters  $\Theta_{\text{V2A}}$ , as illustrated in Fig. 5. The network is trained by minimizing the discrepancy between the synthesized audio and the ground-truth audio, which can be expressed as

$$\hat{\Theta}_{\text{V2A}} = \underset{\Theta_{\text{V2A}}}{\text{argmin}} \left( \|\hat{\mathbf{P}} - \mathbf{P}\|_2^2 + \|\hat{\mathbf{E}} - \mathbf{E}\|_2^2 + \|\hat{\mathbf{F}} - \mathbf{F}\|_F^2 \right), \quad (23)$$

where  $\mathbf{P}$ ,  $\mathbf{E}$ , and  $\mathbf{F}$  denote the ground-truth audio's pitch, energy, and Mel-spectrogram, while  $\hat{\mathbf{P}}$ ,  $\hat{\mathbf{E}}$ , and  $\hat{\mathbf{F}}$  are the predicted features.  $\|\cdot\|_2$  and  $\|\cdot\|_F$  represent the Euclidean norm and Frobenius norm, respectively.

#### D. Semantic Knowledge Base Update Mechanism

Current image-to-video generation semantic transmission frameworks typically rely on a single reference frame as a static shared knowledge base to provide appearance priors. While this ensures a certain degree of appearance consistency, it fails to adapt to variations such as pose changes, illumination shifts, or background transitions. As generation progresses, the initial reference frame often becomes inconsistent with the current content. Consequently, relying on an outdated knowledge base leads to significant distortion and quality degradation. However, in satellite scenarios, frequent updates involving high dimensional image data impose a heavy burden on limited bandwidth and may introduce significant latency.

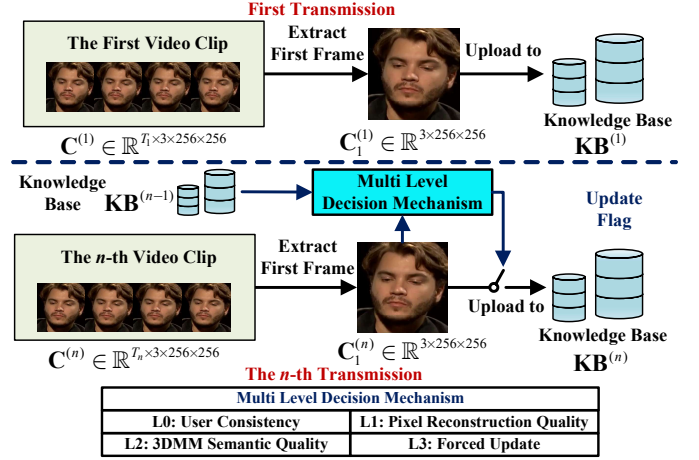


Fig. 6. Process of knowledge base update mechanism.

To address these issues, we propose an adjustable shared knowledge base construction and update mechanism that transmits new reference frames only when significant differences are detected, thereby optimizing satellite resource usage, as illustrated in Fig. 6. Let  $\mathbf{C} = [\mathbf{C}^{(1)}, \mathbf{C}^{(2)}, \dots, \mathbf{C}^{(N)}]$  represent a user multi-segment video collection, where the  $n$ th segment  $\mathbf{C}^{(n)}$  contains  $T_n$  frames. Initially, the first frame  $\mathbf{C}_1^{(1)}$  of the first segment  $\mathbf{C}^{(1)}$  is designated as the reference frame and bound to a user ID to initialize  $\mathbf{KB}^{(1)}$  at both the transmitter and receiver. During decoding, the receiver retrieves this image via the user ID to guide the video synthesis process.

For the  $n$ th segment  $\mathbf{C}^{(n)}$ , the system evaluates differences between its first frame  $\mathbf{C}_1^{(n)}$  and the reference images stored in the current  $\mathbf{KB}^{(n-1)}$  to determine whether an update is required. To ensure efficiency and robustness, a multi-level decision mechanism is designed to evaluate identity consistency, low-level visual quality, and 3DMM semantic consistency.

1) **L0: User Consistency Level:** To maintain identity stability, this level evaluates reference frames in a face embedding space across different video segments. Specifically, the cosine similarity of identity embeddings (CSIM) [76] is calculated to assess the similarity between the initial frame  $\mathbf{C}_1^{(n)}$  of the current segment and the  $i$ th reference image  $\mathbf{I}_i$  in the knowledge base, given by

$$\text{CSIM}_i = \frac{F(\mathbf{C}_1^{(n)}) \cdot F(\mathbf{I}_i)}{\|F(\mathbf{C}_1^{(n)})\| \cdot \|F(\mathbf{I}_i)\|}, \quad i \in \{1, 2, \dots, k\}, \quad (24)$$

where  $F(\cdot)$  denotes the face embedding model,  $\|\cdot\|$  represents the vector norm, and  $k$  is the total number of images stored in the knowledge base.

Let  $\text{CSIM}_i$  denote the maximum similarity between the current frame and all reference images in the knowledge base. If  $\text{CSIM}_i$  exceeds the threshold  $\alpha_{\text{CSIM}}$ , the system considers the current frame sufficiently similar to  $\mathbf{I}_i$  and reuses  $\mathbf{I}_i$  for video generation. Otherwise,  $\mathbf{C}_1^{(n)}$  is appended to the knowledge base as a new reference frame.

2) **L1: Pixel Reconstruction Quality Level:** This level evaluates low-level visual consistency, such as brightness and

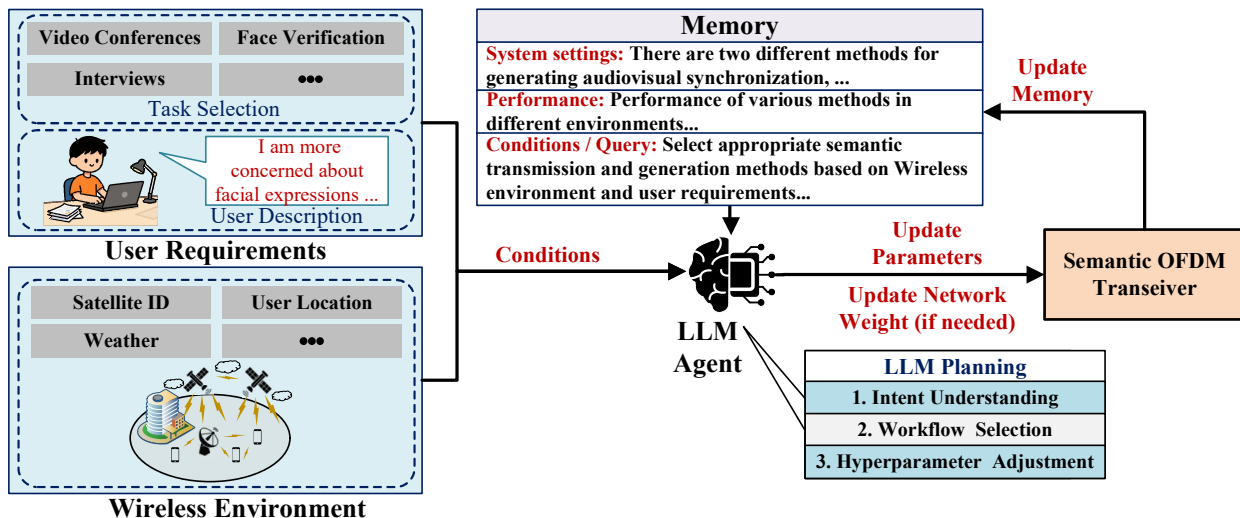


Fig. 7. Adaptive task- and environment-aware strategy based on an LLM agent.

texture, using the peak signal-to-noise ratio (PSNR), which is computed as

$$\text{PSNR}_i = 10 \log_{10} \left( \frac{255^2}{\text{MSE}(\mathbf{C}_1^{(n)}, \mathbf{I}_i)} \right), \quad i \in \{1, 2, \dots, k\}, \quad (25)$$

where  $\text{MSE}(\cdot)$  denotes the MSE.

Let  $\mathbf{I}_i$  be the reference image that maximizes PSNR with respect to  $\mathbf{C}_1^{(n)}$ . Provided that the L0 condition is satisfied, the system compares  $\text{PSNR}_i$  with the threshold  $\alpha_{\text{PSNR}}$  in dB. If  $\text{PSNR}_i > \alpha_{\text{PSNR}}$ ,  $\mathbf{I}_i$  is reused as the reference frame. Otherwise,  $\mathbf{C}_1^{(n)}$  is added to the knowledge base.

3) **L2: 3DMM Semantic Quality Level:** This level evaluates three-dimensional geometric discrepancies, including pose, expression, and translation. Using 3DMM fitting, the system extracts 3D parameters and quantifies the disparity between the current frame and reference images. The weighted 3DMM parameter distance between  $\mathbf{I}_i$  and  $\mathbf{C}_1^{(n)}$  is defined as

$$d_i = \lambda_{\text{exp}} d_{i,\text{exp}} + \lambda_{\text{rot}} d_{i,\text{rot}} + \lambda_{\text{trans}} d_{i,\text{trans}}, \quad (26)$$

where  $d_{i,\text{exp}} = \|\delta_{\text{exp}}^{\mathbf{C}_1^{(n)}} - \delta_{\text{exp}}^{\mathbf{I}_i}\|$ ,  $d_{i,\text{rot}} = \|\delta_{\text{rot}}^{\mathbf{C}_1^{(n)}} - \delta_{\text{rot}}^{\mathbf{I}_i}\|$ , and  $d_{i,\text{trans}} = \|\delta_{\text{trans}}^{\mathbf{C}_1^{(n)}} - \delta_{\text{trans}}^{\mathbf{I}_i}\|$ , with weighting factors  $\lambda_{\text{exp}}$ ,  $\lambda_{\text{rot}}$ , and  $\lambda_{\text{trans}}$ .

Let  $d_i$  be the minimum distance among all reference images. Provided that both L0 and L1 conditions are satisfied, the system verifies whether  $d_{i,\text{exp}} < \alpha_{\text{exp}}$ ,  $d_{i,\text{rot}} < \alpha_{\text{rot}}$ , and  $d_{i,\text{trans}} < \alpha_{\text{trans}}$ . If all conditions are met,  $\mathbf{I}_i$  is reused. Otherwise,  $\mathbf{C}_1^{(n)}$  is added to the knowledge base.

4) **L3: Forced Update Level:** This level assumes sufficient available bandwidth. The system bypasses all similarity evaluations and directly adds  $\mathbf{C}_1^{(n)}$  to the knowledge base as a new reference frame for each segment. Although this strategy maximizes reconstruction quality and temporal consistency, it incurs significantly higher bandwidth overhead.

### E. LLM Agent Based Environment and Task Adaptability

Although the proposed dual-stream generation framework and knowledge base update mechanism provide adaptability to user and scenario requirements, real-time configuration adjustment remains challenging due to fluctuating channel conditions and varying task types. In complex environments characterized by high-mobility dynamics and rain attenuation, static configurations often fail to ensure optimal performance. To address this limitation, we propose a system capable of automatically generating optimized configuration schemes and workflows tailored to channel environments, satellite-to-ground bandwidth constraints, and user requirements.

Conventional rule-based or lookup-table methods are effective in simple scenarios but suffer from combinatorial explosion as task diversity increases, making maintenance and scalability difficult. Moreover, these methods often fail to capture the semantic intent underlying different tasks. In contrast, LLMs possess inherent semantic understanding and autonomous planning capabilities, enabling effective interaction with both users and the environment. Therefore, an LLM-based agent is introduced for adaptive semantic transmission decision making in satellite communication systems. This agent enables the dynamic selection of semantic strategies and bandwidth configurations based on multidimensional environmental information and user requirements.

During the initialization phase, the LLM agent is configured through prompt engineering or fine-tuning. It analyzes system configurations and historical transmission logs, such as satellite identifiers, orbital positions, and weather conditions, as well as the performance of different semantic strategies. By learning the mapping between wireless environments and task performance, the agent constructs an initial memory base to support subsequent decision making.

During operation, the agent processes inputs including task descriptions, user preferences, such as quality priority, and real-time environmental data. It then executes a three-step reasoning and planning procedure.

TABLE II  
SYSTEM PARAMETERS

Parameter	Value
Transmit Power ( $P_t$ )	25 dBm
Transmit Antenna Gain ( $G_t$ )	40 dBi
Satellite Equivalent Gain ( $G_s$ )	85 dBi
Receive Antenna Gain ( $G_r$ )	40 dBi
Boltzmann Constant ( $k$ )	1.38e-23 J/K
Noise Temperature ( $T$ )	290 K
System Bandwidth ( $B$ )	20 MHz

- **Intent understanding:** The agent analyzes task objectives and performance requirements while incorporating environmental information to assess the current satellite link quality.
- **Workflow selection:** Based on the inferred context, the agent selects the most suitable workflow from the supported generation workflows and semantic transmission strategies.
- **Resource and hyperparameter adjustment:** The agent dynamically adjusts hyperparameters, including the semantic feature compression rate, bandwidth allocation, and the activation of knowledge base updates, to ensure task completion.

The resulting plan directly configures the satellite OFDM transceiver. After task completion, the system records the full transmission context in the memory base. If the LLM detects configuration inadequacy during inference, it generates new candidate schemes. Once verified, these schemes are incorporated into the configuration set, enabling the system to continuously evolve and adapt to diverse service scenarios.

## V. NUMERICAL RESULTS

In this section, we present a performance and bandwidth consumption comparison between the proposed system and existing audio and video transmission methods. Experiments were conducted utilizing the LRS2 [77] and VoxCeleb [78] datasets, which comprise time-aligned talking-head videos. The videos were resized to a resolution of  $256 \times 256$ . The training set consists of 40,000 audiovisual pairs from LRS2, while the test set includes an additional 8,000 audiovisual pairs from LRS2 and a subset of the VoxCeleb dataset.

To simulate the satellite environment, we employed the NTN-TDL-A channel model. The satellite altitude was randomly selected from the range of 300 km to 1,200 km, and the ground terminal’s movement speed is set to 3 km/h. The physical layer OFDM system comprised 14 symbols per frame and 120 subcarriers. A comb-type pilot pattern was implemented with a spacing of 4 subcarriers. Therefore, 30 subcarriers were allocated for pilots and 90 for data transmission. Other system parameters are shown in Table II.

### A. Network Setting and Benchmarks

The deployment and training strategies for the framework’s modules are detailed as follows:

TABLE III  
COMPUTATIONAL COMPLEXITY AND TRANSMISSION BANDWIDTH

Type	Method	Transmission Symbols	Params [M]	Runtime [s]
Video Level	H264+LDPC	400,991	–	0.33e-1
	H265+LDPC	54,390	–	0.13e-1
	SVC	600	60.11	0.19e-1
	V2A (Video Part)	300	172.01	0.71e-1
	A2V (Video Part)	0	159.88	0.53e-1
Audio Level	FastSpeech 2	600	70.46	0.19e-1
	DeepSC-S	32,768	0.75	0.21e-2
	V2A (Audio Part)	300	368.89	0.10e-0
	A2V (Audio Part)	600	317.25	0.65e-1

- **Semantic extraction module:** Comprising 3DMM extraction, speech recognition, and acoustic information extraction networks, these pre-trained models are deployed directly at the transmitter.
- **Semantic encoder and decoder:** Distinct encoder-decoder networks are established for each semantic feature type (3DMM, text, phonemes, duration). These networks are trained under noisy satellite channels to minimize transmission error, following (15).
- **Multimodal reconstruction module:** The modules  $f_{VG}(\cdot)$ ,  $f_{A2M}(\cdot)$ ,  $f_{Mel}(\cdot)$ ,  $f_{HiFi}(\cdot)$ , and  $f_{Lip}(\cdot)$  utilize pre-trained weights from large-scale audiovisual datasets, which demonstrate robust performance. Conversely, the lip-to-Mel-spectrogram generator  $f_{V2A}(\cdot)$  requires specific training via (23), to mitigate channel noise and ensure audiovisual synchronization, conditioned on the generated video  $\hat{V}$  and received text.
- **LLM agent:** The system utilizes GPT-4o [24] as the decision-making agent, employing its advanced task comprehension and reasoning capabilities to control system operations.

All networks requiring training utilized the Adam optimizer. Specifically, the four semantic encoder-decoder pairs were trained for 400 epochs with a learning rate of 0.001, while the  $f_{V2A}(\cdot)$  was trained for 1000 epochs with a learning rate of 0.0001. The parameters for semantic knowledge base update mechanism are set to  $\alpha_{CSIM} = 0.7$ ,  $\alpha_{PSNR} = 13$ ,  $\alpha_{exp} = 8$ ,  $\alpha_{rot} = 0.3$ ,  $\alpha_{trans} = 0.3$ ,  $\lambda_{exp} = 0.1$ ,  $\lambda_{rot} = 1$ , and  $\lambda_{trans} = 1$ .

To compare performance, for video modality, we used H264/H265 with LDPC coding and 64 quadrature amplitude modulation (64-QAM) as traditional baselines, while SVC [17] based on video keypoint transmission and generation is used as the semantic video baseline. For the audio modality, the end-to-end waveform encoding and decoding method DeepSC-S [79] was used as the baseline for semantic audio transmission, and the text-to-audio generation network FastSpeech 2 [71] was employed as the baseline for audiovisual synchronization.

Table III details the complexity and bandwidth metrics, evaluated on an Intel i9-14900k CPU and an Nvidia RTX 4090 GPU, with runtime measured per frame for video and per clip for audio. In terms of runtime and parameters, traditional H265 and the lightweight semantic communication model (DeepSC-S) exhibit low inference latency, as they do not involve large-scale generative networks. In contrast, the V2A and A2V algorithms, which integrate semantic extraction and cross-modal

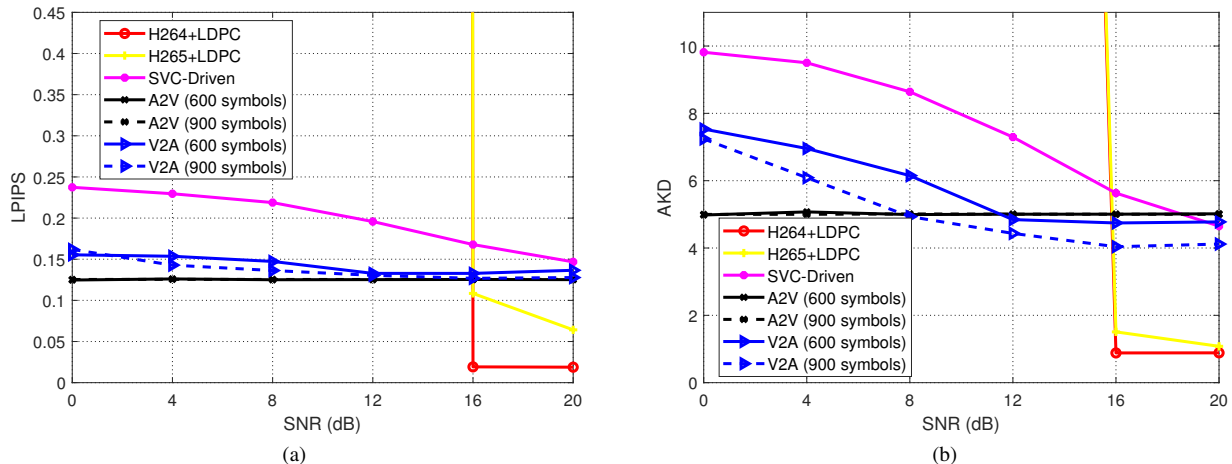


Fig. 8. Performance of different video transmission methods under varying SNR conditions. (a) LPIPS performance; (b) AKD performance.

generative networks, incur higher inference latency. However, in terms of transmission bandwidth, V2A and A2V demonstrate superior bandwidth efficiency, achieving several orders of magnitude higher compression than H265 and DeepSC-S via cross-modal semantic generation. Notably, A2V achieves “zero-symbol” video transmission, synthesizing video content solely from audio semantics without requiring video semantic transmission. In conclusion, while the proposed methods increase computational load, their substantial bandwidth savings offer clear benefits for narrowband satellite communication. Future optimization (e.g., pruning, quantization) can further balance computational and transmission efficiency.

The performance of the multimodal semantic transmission is evaluated across three dimensions: video reconstruction, audio reconstruction, and audiovisual synchronization.

- **Video reconstruction:** Video quality is assessed using the CSIM [76] for identity consistency and the learned perceptual image patch similarity (LPIPS) [80] for perceptual discrepancy based on deep features. Given the focus on facial video, average keypoint distance (AKD) [81] is employed to evaluate the accuracy of facial motion and expression. Here, higher CSIM and lower LPIPS or AKD indicate better quality.
- **Audio reconstruction:** Evaluation considers both intelligibility and perceptual quality. Word error rate (WER) measures the accuracy of textual semantics. Perceptual quality is assessed via perceptual evaluation of speech quality (PESQ) [82], an ITU-T P.862 standard evaluating audio clarity and naturalness. Lower WER and higher PESQ are preferred.
- **Audiovisual synchronization:** We employ lip-sync error distance (LSE-D) and lip-sync error confidence (LSE-C) [83] to quantify lip-synchronization performance. LSE-D measures the temporal mismatch between lip movements and audio, while LSE-C evaluates synchronization reliability through confidence scores. Lower LSE-D and higher LSE-C denote better synchronization.

### B. Semantic Transmission Performance

This section evaluates the system performance in terms of video fidelity, audio quality, and audiovisual synchronization. Fig. 8 compares video transmission methods using LPIPS and AKD. As shown in Fig. 8(a), under high SNR, traditional H264/H265 achieve lower LPIPS but require significantly higher bandwidth. However, under low SNR, traditional methods suffer from rapid performance degradation, whereas generative methods (A2V and V2A) exhibit superior robustness. The AKD results in Fig. 8(b) confirm this trend. While traditional methods excel only at high SNR, V2A maintains stable keypoint reconstruction even at low SNR, underscoring its capability in preserving video semantics.

To evaluate the impact of bandwidth on performance, we set the total bandwidth for A2V and V2A to 600 and 900 symbols. In both cases, 300 symbols are allocated to text, while the remaining bandwidth is used for video or audio features. With increased bandwidth, V2A (900 symbols) significantly improves AKD compared to V2A (600 symbols), demonstrating that higher bandwidth enhances video semantic reconstruction. In contrast, A2V, which only transmits audio semantics and drives video generation through audio, performs well under bandwidth constraints or poor channel conditions. However, it exhibits a performance bottleneck, where additional bandwidth does not further enhance video reconstruction.

Fig. 9 shows reconstructed video frames and AKD performance at 12 dB SNR. The results show that V2A, by transmitting video semantics, achieves superior reconstruction of video semantics. In contrast, A2V is limited by its audio-driven video generation nature. SVC relies on geometric keypoints, which are extremely sensitive to channel noise. Even minor interference can lead to significant facial misalignment. In contrast, traditional methods fail to reconstruct recognizable content under the dual constraints of limited bandwidth and severe noise.

Table IV evaluates audio transmission methods at 20 dB SNR. The LSE-C and LSE-D are based on a comparison between the transmitted audio and the original video, with the original audio serving as the ground truth. DeepSC-

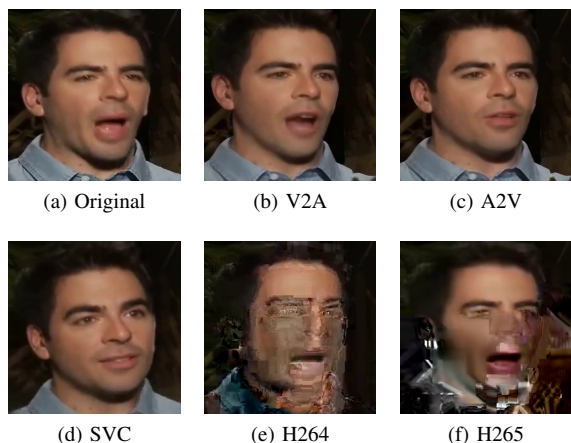


Fig. 9. Reconstruction results of various methods under SNR = 12 dB. (a) Original image; (b) V2A (AKD = 5.41); (c) A2V (AKD = 5.85); (d) SVC (AKD = 8.36); (e) H264 (AKD = N/A); (f) H265 (AKD = N/A). N/A indicates that the keypoints cannot be detected to calculate AKD because the face is blurred.

TABLE IV  
AUDIO TRANSMISSION PERFORMANCE OF DIFFERENT METHODS

Method	LSE-C	LSE-D	WER	PESQ
Original Audio	8.33	6.07	0.036	4.50
DeepSC-S	7.85	6.57	0.11	2.99
A2V	5.85	8.69	0.11	1.25
V2A	2.22	12.16	0.11	1.18
FastSpeech 2	3.12	10.21	0.079	1.15

S maintains high quality but consumes approximately  $28\times$  the bandwidth of generative methods. A2V, by transmitting additional semantics such as duration, achieves synchronization scores comparable to DeepSC-S with minimal overhead. Meanwhile, FastSpeech 2 and V2A show a marginal decline in synchronization due to the absence of acoustic characteristics. It is also observed that FastSpeech2 achieves the lowest WER by allocating the highest bandwidth to text.

Fig. 10(a) and (b) illustrate audiovisual synchronization performance. 3DMM and SVC, which generate video based on geometric parameters or keypoints, exhibit a low match with the original audio, resulting in poorer performance. In contrast, the cross-modal generative methods (A2V and V2A) demonstrate superior synchronization, with performance improving consistently as bandwidth increases.

In summary, V2A prioritizes video semantic transmission, yielding significant quality gains with increased bandwidth, while A2V excels in audio-related semantic modeling. Therefore, in subsequent application stages, the proposed system can dynamically select the optimal transmission path based on channel conditions and task requirements, making it highly effective for narrowband satellite communication scenarios.

### C. Impact of Knowledge Base on Semantic Method Performance

The quality of the shared knowledge base significantly influences generative performance. To assess the proposed update mechanisms, we conducted experiments in scenarios involving the transmission of 100 video segments with multiple users, measuring CSIM, LPIPS, and AKD, as shown in Fig. 11. We

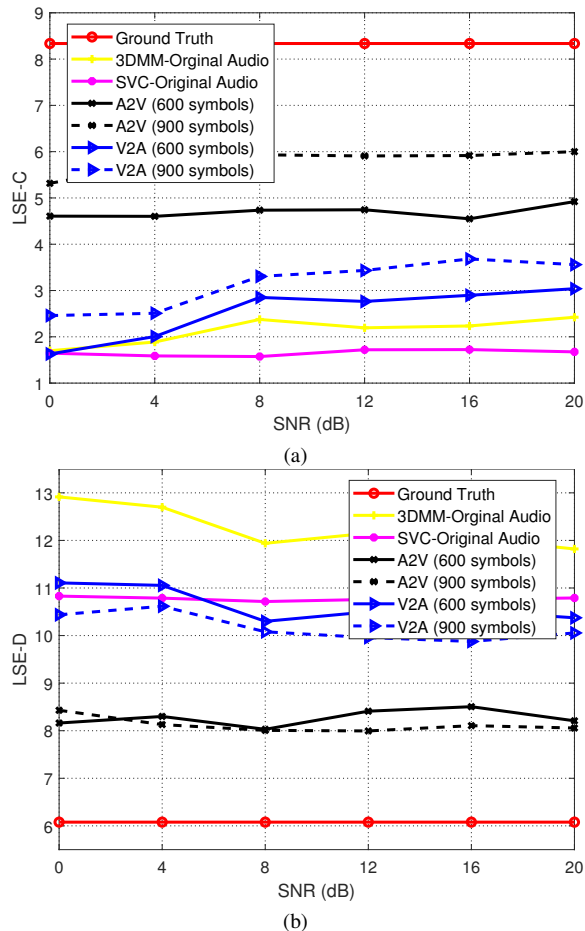


Fig. 10. Audiovisual synchronization performance of different transmission methods. (a) LSE-C performance; (b) LSE-D performance.

TABLE V  
AVERAGE TRANSMISSION BANDWIDTH PER VIDEO ACROSS DIFFERENT KNOWLEDGE BASE UPDATE LEVELS

Update Level	Update Count	Semantic Symbols	Knowledge Base Update Symbols
L0	17	300	2,785
L1	27	300	4,427
L2	50	300	8,192
L3	100	300	16,384

compare the proposed L0-L2 against a baseline L3 (which updates the reference frame for every segment). Table V shows the average bandwidth overhead for each level, where the semantic features (3DMM parameters or keypoints) have a fixed bandwidth, and user image updates in the knowledge base employ a JSCC image transmission method [12] with a compression rate of  $1/12$ , transmitted over a high-quality channel. The transmission of a  $256\times 256\times 3$  image requires 16,384 symbols.

These results demonstrate that performance gradually improves as the judgment criteria become more stringent. Specifically, L0 (identity-only) maintains  $CSIM > 0.7$ , ensuring basic identity recognition, but performs poorly in texture details and geometric accuracy, resulting in mediocre LPIPS and AKD scores. Integrating pixel-level (L1) and semantic-

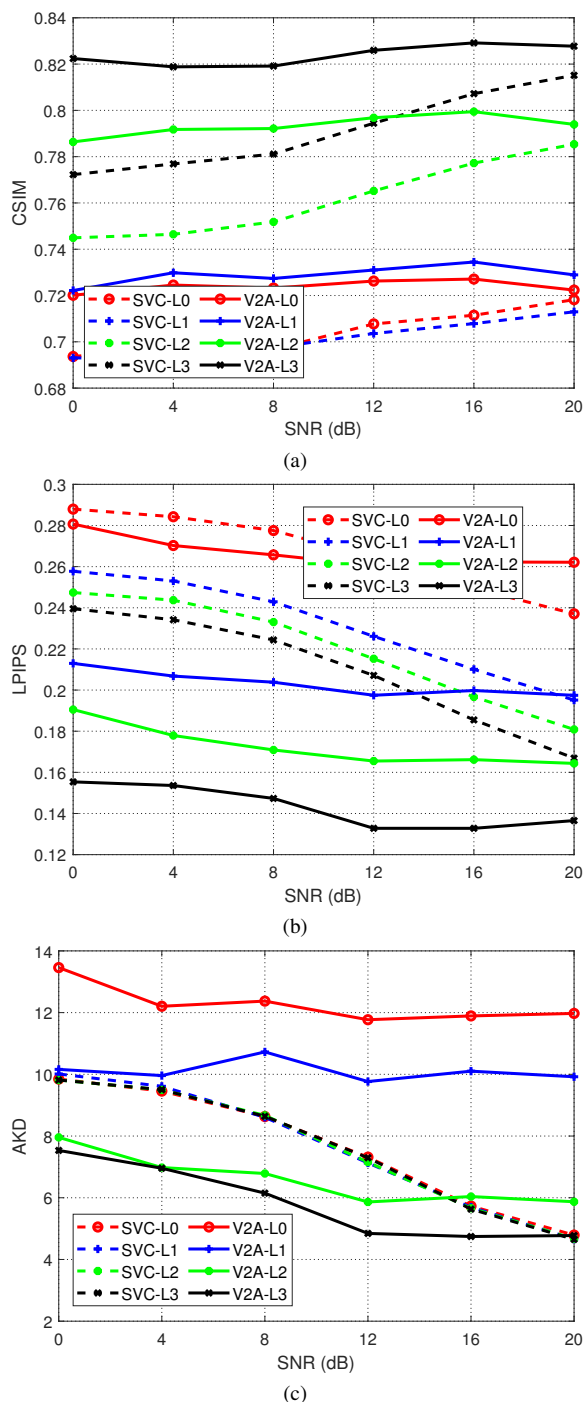


Fig. 11. Impact of knowledge base update levels on different semantic transmission methods. (a) CSIM performance; (b) LPIPS performance; (c) AKD performance.

level (L2) constraints significantly enhances reconstruction accuracy for both SVC and V2A. In contrast, L3 shows slight advantages across all metrics, but its update frequency and bandwidth consumption increase dramatically. In satellite links characterized by high latency and error rates, such frequent high-volume transmissions pose a risk of link congestion and reliability issues, leading to deployment bottlenecks. Notably, V2A-L2 closely approximates the performance of V2A-L3. For example, at 12 dB SNR, V2A-L2 achieves an AKD of 5.8,

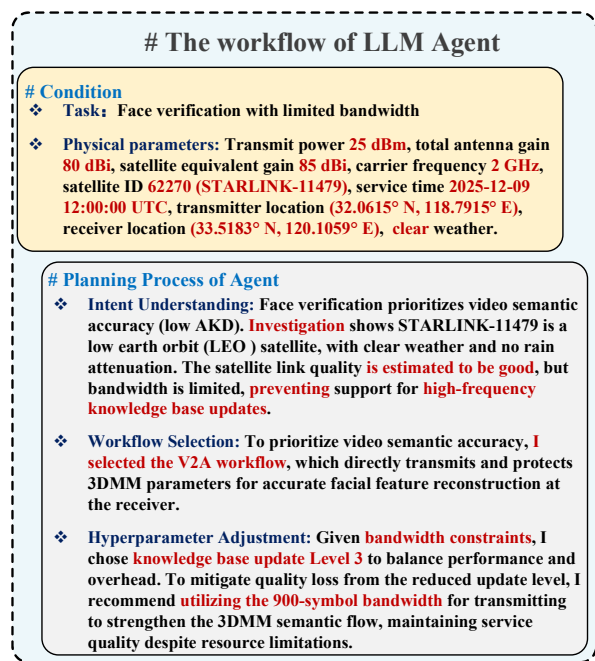


Fig. 12. Decision Process of LLM agent in bandwidth-constrained facial verification task.

comparable to the 4.8 of L3, while consuming only about 50% of the bandwidth required by L3. This demonstrates that the proposed mechanism effectively balances generation quality with resource conservation, ensuring stable and cost-effective multimodal transmission in bandwidth-limited satellite environments.

#### D. Case Study on Task and Environment Adaptability

This case study evaluates the practical deployment of the LLM agent, utilizing the simulation results from previous sections as the agent's long-term memory. The agent's performance is compared with the traditional "Lookup-Table" method, which operates via static, rule-based queries of historical performance data. The agent's reasoning process for a face-verification task is detailed in Fig. 12. The simulation scenario is defined by a transmit power of 25 dBm, total antenna gains of 80 dBi, a satellite equivalent gain of 85 dBi, and a 2 GHz carrier frequency, serviced by STARLINK-11479 (ID 62270). The evaluation period is centered around 2025-12-09 12:00:00 (UTC) for the transmitter at (32.0615° N, 118.7915° E) and the receiver at (33.5183° N, 120.1059° E) during clear weather.

Upon receiving these inputs, the agent first analyzes the task and scenario, recognizing the high video semantic accuracy requirement for face verification. By evaluating the physical parameters, the agent assesses the link quality as good but identifies "bandwidth limitation" as a core constraint, which restricts frequent knowledge base updates. Therefore, the agent selects the V2A workflow to prioritize direct transmission and protection of 3DMM parameters, ensuring accurate facial reconstruction. To optimize resource usage, it downshifts from the high-cost L3 update scheme to the more balanced L2. Additionally, the saved bandwidth is reallocated to preserve

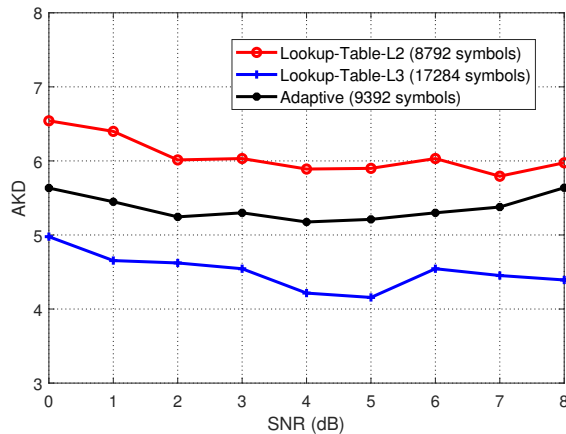


Fig. 13. Performance of different strategies during the service time.

the accuracy of 3DMM semantics, thereby mitigating potential quality loss and ensuring service quality within resource limits.

Fig. 13 shows the AKD performance of different strategies over several 20-second intervals near the service time (2025-12-09 12:00:00 UTC), reflecting link quality variations caused by satellite mobility. While the “Lookup-Table” method also identifies the V2A workflow as optimal through historical querying, its execution remains inflexible. As shown, while the Lookup-Table-L3 variant achieves peak AKD performance, it does so at the cost of continuous, high-frequency knowledge base updates (totaling 17,284 symbols per segment). In contrast, the proposed adaptive strategy actively reduces the update level and reallocates bandwidth to enhance semantic protection. This strategy achieves performance comparable to Lookup-Table-L3 while consuming approximately 50% less bandwidth. Meanwhile, Lookup-Table-L2, with a similar bandwidth allocation, consistently performs worse due to its lack of environmental understanding and dynamic planning capabilities.

In summary, this case study demonstrates that the proposed adaptive decision-making framework deeply integrates environmental awareness, task understanding, and resource planning. Through system-level resource coordination and optimization, it effectively balances semantic fidelity and transmission overhead under stringent bandwidth constraints, significantly enhancing the overall robustness and resource efficiency of the system.

## VI. CONCLUSION

This paper proposes an adaptive multimodal semantic transmission system for satellite communications, addressing the limitation of rigid transmission rules under highly uncertain channel conditions. Unlike traditional methods that rely on fixed modal priorities, our system employs a dual-stream architecture capable of flexibly switching between video-driven and audio-driven generation paths, thereby ensuring task adaptability in complex scenarios. To optimize the trade-off between knowledge base maintenance costs and generation quality, a dynamic keyframe update mechanism is introduced. This mechanism maintains the knowledge base as needed, achieving

a balance between generation quality and bandwidth consumption. Crucially, an intelligent decision module is developed by leveraging an LLM agent to orchestrate these components. By reasoning over wireless conditions and task requirements, this module replaces static heuristics with active transmission strategies, solving complex decision-making problems in constrained environments. Simulation results demonstrate the superiority of integrating cross-modal generation with intelligent management in satellite links. This architecture provides a robust foundation for next-generation multimedia satellite networks, enabling high-fidelity communication in resource-limited environments.

## REFERENCES

- [1] B. Di, L. Song, Y. Li, and H. V. Poor, “Ultra-dense LEO: Integration of satellite access networks into 5G and beyond,” *IEEE Wireless Commun.*, vol. 26, no. 2, pp. 62–69, Apr. 2019.
- [2] O. Kodheli, E. Lagunas, N. Maturo, S. K. Sharma, B. Shankar, Montoya *et al.*, “Satellite communications in the new space era: A survey and future challenges,” *IEEE Commun. Surv. Tutor.*, vol. 23, no. 1, pp. 70–109, Oct. 2021.
- [3] N. Saeed, A. Elzanaty, H. Almorad, H. Dahrouj, T. Y. Al-Naffouri, and M.-S. Alouini, “Cubesat communications: Recent advances and future challenges,” *IEEE Commun. Surv. Tutor.*, vol. 22, no. 3, pp. 1839–1862, Apr. 2020.
- [4] Y. Su, Y. Liu, Y. Zhou, J. Yuan, H. Cao, and J. Shi, “Broadband leo satellite communications: Architectures and key technologies,” *IEEE Wireless Commun.*, vol. 26, no. 2, pp. 55–61, Apr. 2019.
- [5] A. Agarwal and P. Kumar, “Analysis of variable bit rate SOFDM transmission scheme over multi-relay hybrid satellite-terrestrial system in the presence of CFO and phase noise,” *IEEE Trans. Vehi. Tech.*, vol. 68, no. 5, pp. 4586–4601, May 2019.
- [6] W. Lu, K. An, T. Liang, and X. Yan, “Robust beamforming in multibeam satellite systems with non-orthogonal multiple access,” *IEEE Wireless Commun. Lett.*, vol. 9, no. 11, pp. 1889–1893, Nov. 2020.
- [7] Z. Qin, X. Tao, J. Lu, W. Tong, and G. Y. Li, “Semantic communications: Principles and challenges,” *arXiv preprint arXiv:2201.01389*, 2021.
- [8] J. Ren, Z. Zhang, J. Xu, G. Chen, Y. Sun, P. Zhang, and S. Cui, “Knowledge base enabled semantic communication: A generative perspective,” *IEEE Wireless Commun.*, vol. 31, no. 4, pp. 14–22, Aug. 2024.
- [9] C. Chaccour, W. Saad, M. Debbah, Z. Han, and H. Vincent Poor, “Less data, more knowledge: Building next-generation semantic communication networks,” *IEEE Commun. Surv. Tutor.*, vol. 27, no. 1, pp. 37–76, Feb. 2025.
- [10] H. Xie and Z. Qin, “A lite distributed semantic communication system for internet of things,” *IEEE J. Sel. Areas Commun.*, vol. 39, no. 1, pp. 142–153, Jan. 2021.
- [11] Q. Zhou, R. Li, Z. Zhao, Y. Xiao, and H. Zhang, “Adaptive bit rate control in semantic communication with incremental knowledge-based HARQ,” *IEEE Open J. Commun. Soc.*, vol. 3, pp. 1076–1089, Jul. 2022.
- [12] E. Boursoulatzé, D. Burth Kurka, and D. Gündüz, “Deep joint source-channel coding for wireless image transmission,” *IEEE Trans. Cognit. Commun. Netw.*, vol. 5, no. 3, pp. 567–579, Sep. 2019.
- [13] J. Xu, B. Ai, W. Chen, A. Yang, P. Sun, and M. Rodrigues, “Wireless image transmission using deep source channel coding with attention modules,” *IEEE Trans. Circuits Syst. Video Technol.*, vol. 32, no. 4, pp. 2315–2328, Apr. 2022.
- [14] T.-Y. Tung and D. Gündüz, “DeepWiVe: Deep-learning-aided wireless video transmission,” *IEEE J. Select. Areas Commun.*, vol. 40, no. 9, pp. 2570–2583, Sep. 2022.
- [15] S. Wang, J. Dai, Z. Liang, K. Niu, Z. Si, C. Dong, X. Qin, and P. Zhang, “Wireless deep video semantic transmission,” *IEEE J. Sel. Areas Commun.*, vol. 41, no. 1, pp. 214–229, Jan. 2023.
- [16] C. Liang, X. Deng, Y. Sun, R. Cheng, L. Xia, D. Niyato, and M. A. Imran, “VISTA: Video transmission over a semantic communication approach,” in *Proc. IEEE Int. Conf. Commun. Workshops (ICC Workshops)*, Rome, Italy, May 2023, pp. 1777–1782.
- [17] P. Jiang, C.-K. Wen, S. Jin, and G. Y. Li, “Wireless semantic communications for video conferencing,” *IEEE J. Sel. Areas Commun.*, vol. 41, no. 1, pp. 230–244, Jan. 2023.

- [18] H. Xie, Z. Qin, X. Tao, and K. B. Letaief, "Task-oriented multi-user semantic communications," *IEEE J. Select. Areas Commun.*, vol. 40, no. 9, pp. 2584–2597, Sep. 2022.
- [19] F. Yu, Z. Xiang, N. Che, Z. Zhang, Y. Li, J. Xue, and Z. Wan, "Pilot-guided multimodal semantic communication for audio-visual event localization," *arXiv preprint arXiv:2412.06208*, 2024.
- [20] Y. Tian, J. Ying, Z. Qin, Y. Jin, and X. Tao, "Synchronous multi-modal semantic communication system with packet-level coding," *IEEE Trans. Wireless Commun.*, vol. 24, no. 5, pp. 3684–3697, May 2025.
- [21] H. Tong, H. Li, H. Du, Z. Yang, C. Yin, and D. Niyato, "Multimodal semantic communication for generative audio-driven video conferencing," *IEEE Wireless Commun. Lett.*, vol. 14, no. 1, pp. 93–97, Jan. 2025.
- [22] P. Tandon, S. Chandak, P. Pataranutaporn, Y. Liu, A. M. Mapuranga, P. Maes, T. Weissman, and M. Sra, "Txt2vid: Ultra-low bitrate compression of talking-head videos via text," *IEEE J. Select. Areas Commun.*, vol. 41, no. 1, pp. 107–118, Jan. 2023.
- [23] F. Jiang, S. Tu, L. Dong, C. Pan, J. Wang, and X. You, "Large generative model-assisted talking-face semantic communication system," *arXiv preprint arXiv:2411.03876*, 2024.
- [24] J. Achiam, S. Adler, S. Agarwal, L. Ahmad, I. Akkaya, F. L. Aleman, D. Almeida, J. Altenschmidt, S. Altman, S. Anadkat *et al.*, "GPT-4 technical report," *arXiv preprint arXiv:2303.08774*, 2023.
- [25] P. Jiang, J. Guo, C.-K. Wen, S. Jin, and J. Zhang, "Semantic communications with world models," *arXiv preprint arXiv:2510.24785*, 2025.
- [26] M. A. Vázquez, A. Perez-Neira, D. Christopoulos, S. Chatzinotas, B. Ottersten, P.-D. Arapoglou, A. Ginesi, and G. Taricco, "Precoding in multibeam satellite communications: Present and future challenges," *IEEE Wireless Commun.*, vol. 23, no. 6, pp. 88–95, Dec. 2016.
- [27] Y. Zhang, Z. Wang, Y. Huang, W. Wei, G. F. Pedersen, and M. Shen, "A digital signal recovery technique using DNNs for LEO satellite communication systems," *IEEE Trans. Ind. Electron.*, vol. 68, no. 7, pp. 6141–6151, Jul. 2021.
- [28] R. Ali Ahmad, J. Lacan, F. Arnal, M. Gineste, and L. Clarac, "Enhancing satellite system throughput using adaptive HARQ for delay tolerant services in mobile communications," in *Proc. Wireless Telecommun. Symp. (WTS)*, New York, NY, USA, Apr. 2015, pp. 1–7.
- [29] M. Hosseinian, J. P. Choi, S.-H. Chang, and J. Lee, "Review of 5G NTN standards development and technical challenges for satellite integration with the 5G network," *IEEE Aerosp. Electron. Syst. Mag.*, vol. 36, no. 8, pp. 22–31, Aug. 2021.
- [30] Y. Qi, H. Deng, M. Liu, and Z. Li, "On the standardization of key enabling technologies in non-terrestrial network air-interface design," in *Proc. IEEE/CIC Int. Conf. Commun. China Workshops (ICCC Workshops)*, Xiamen, China, Jul. 2021, pp. 343–348.
- [31] F. Fourati and M.-S. Alouini, "Artificial intelligence for satellite communication: A review," *Intell. Conver. Netw.*, vol. 2, no. 3, pp. 213–243, Sep. 2021.
- [32] G. Zheng, Q. Ni, K. Navaie, and H. Pervaiz, "Semantic communication in satellite-borne edge cloud network for computation offloading," *IEEE J. Sel. Areas Commun.*, vol. 42, no. 5, pp. 1145–1158, May 2024.
- [33] Y. Yin, S. Liu, D. Wen, Y. Wu, and Y. Shi, "Joint source and channel coding for multi-modal satellite-to-ground semantic communications," in *Proc. IEEE Wireless Commun. Netw. Conf. (WCNC)*, Milan, Italy, Mar. 2025, pp. 1–6.
- [34] H. Xie, Z. Qin, G. Y. Li, and B.-H. Juang, "Deep learning based semantic communications: An initial investigation," in *Proc. IEEE Global Commun. Conf. (GLOBECOM)*, Taipei, Taiwan, Dec. 2020, pp. 1–6.
- [35] J. Bao, P. Basu, M. Dean, C. Partridge, A. Swami, W. Leland, and J. A. Hendler, "Towards a theory of semantic communication," in *Proc. IEEE Netw. Sci. Workshop (NSW)*, West Point, NY, USA, Jun. 2011, pp. 110–117.
- [36] C. Bian, Y. Shao, and D. Gündüz, "DeepJSCC-I++: Robust and bandwidth-adaptive wireless image transmission," in *Proc. IEEE Global Commun. Conf. (GLOBECOM)*, Kuala Lumpur, Malaysia, Dec. 2023, pp. 3148–3154.
- [37] M. Yang, C. Bian, and H.-S. Kim, "OFDM-guided deep joint source channel coding for wireless multipath fading channels," *IEEE Trans. Cogn. Commun. Netw.*, vol. 8, no. 2, pp. 584–599, Jun. 2022.
- [38] H. Wu, Y. Shao, C. Bian, K. Mikolajczyk, and D. Gündüz, "Deep joint source-channel coding for adaptive image transmission over MIMO channels," *IEEE Trans. Wireless Commun.*, vol. 23, no. 10, pp. 15002–15017, Oct. 2024.
- [39] H. Xie, Z. Qin, G. Y. Li, and B.-H. Juang, "Deep learning enabled semantic communication systems," *IEEE Trans. Signal Process.*, vol. 69, pp. 2663–2675, Apr. 2021.
- [40] Z. Weng, Z. Qin, and G. Y. Li, "Semantic communications for speech signals," in *Proc. IEEE Int. Conf. Commun. (ICC)*, Montreal, QC, Canada, Jun. 2021, pp. 1–6.
- [41] J. Guo, Y. Zhang, C. Liu, W. Xu, and Z. Bie, "SNR-adaptive multi-layer semantic communication for speech," in *Proc. IEEE Annu. Int. Symp. Pers., Indoor, Mobile Radio Commun. (PIMRC)*, Toronto, ON, Canada, Sep. 2023, pp. 1–6.
- [42] X. Liu, H. Liang, Z. Bao, C. Dong, and X. Xu, "A semantic communication system for point cloud," *IEEE Trans. Veh. Technol.*, vol. 74, no. 1, pp. 894–910, Jan. 2025.
- [43] A. Creswell, T. White, V. Dumoulin, K. Arulkumaran, B. Sengupta, and A. A. Bharath, "Generative adversarial networks: An overview," *IEEE Signal Process. Mag.*, vol. 35, no. 1, pp. 53–65, Jan. 2018.
- [44] R. Rombach, A. Blattmann, D. Lorenz, P. Esser, and B. Ommer, "High-resolution image synthesis with latent diffusion models," in *Proc. IEEE/CVF Conf. Comput. Vis. Pattern Recognit. (CVPR)*, New Orleans, Louisiana, Jan. 2022, pp. 10684–10695.
- [45] A. Liu, B. Feng, B. Xue, B. Wang, B. Wu, C. Lu, C. Zhao, C. Deng, C. Zhang, C. Ruan *et al.*, "Deepseek-v3 technical report," *arXiv preprint arXiv:2412.19437*, 2024.
- [46] Z. Weng, Z. Qin, and G. Y. Li, "Semantic communications for speech recognition," in *Proc. IEEE Global Commun. Conf. (GLOBECOM)*, Madrid, Spain, Dec. 2021, pp. 1–6.
- [47] Z. Weng, Z. Qin, X. Tao, C. Pan, G. Liu, and G. Y. Li, "Deep learning enabled semantic communications with speech recognition and synthesis," *IEEE Trans. Wireless Commun.*, vol. 22, no. 9, pp. 6227–6240, Sep. 2023.
- [48] T. Han, Q. Yang, Z. Shi, S. He, and Z. Zhang, "Semantic-preserved communication system for highly efficient speech transmission," *IEEE J. Sel. Areas Commun.*, vol. 41, no. 1, pp. 245–259, Jan. 2023.
- [49] J. Shen, R. Pang, R. J. Weiss, M. Schuster, N. Jaitly, Z. Yang, Z. Chen, Y. Zhang, Y. Wang, R. Skerrv-Ryan, R. A. Saurous, Y. Agiomvrgianakis, and Y. Wu, "Natural TTS synthesis by conditioning wavenet on mel spectrogram predictions," in *Proc. IEEE Int. Conf. Acoust., Speech Signal Process. (ICASSP)*, Calgary, AB, Canada, Apr. 2018, pp. 4779–4783.
- [50] J. Shao, J. Tong, Q. Wu, W. Guo, Z. Li, Z. Lin, and J. Zhang, "WirelessLLM: Empowering large language models towards wireless intelligence," *J. Commun. Inf. Netw.*, vol. 9, no. 2, pp. 99–112, Jun. 2024.
- [51] F. Jiang, Y. Peng, L. Dong, K. Wang, K. Yang, C. Pan, D. Niyato, and O. A. Dobre, "Large language model enhanced multi-agent systems for 6g communications," *IEEE Wireless Commun.*, vol. 31, no. 6, pp. 48–55, Dec. 2024.
- [52] A. Kirillov, E. Mintun, N. Ravi, H. Mao, C. Rolland, L. Gustafson, T. Xiao, S. Whitehead, A. C. Berg, W.-Y. Lo *et al.*, "Segment anything," in *Proc. IEEE/CVF Int. Conf. Comput. Vis.*, Paris, France, Oct. 2023, pp. 4015–4026.
- [53] S. Tariq, B. E. Arfeto, C. Zhang, and H. Shin, "Segment anything meets semantic communication," *arXiv preprint arXiv:2306.02094*, 2023.
- [54] G. Cicchetti, E. Grassucci, J. Park, J. Choi, S. Barbarossa, and D. Cominiello, "Language-oriented semantic latent representation for image transmission," in *Proc. IEEE 34th Int. Workshop Mach. Learn. Signal Process. (MLSP)*, London, United Kingdom, Sep. 2024, pp. 1–6.
- [55] W. Chen, W. Xu, H. Chen, X. Zhang, Z. Qin, Y. Zhang, and Z. Han, "Semantic communication based on large language model for underwater image transmission," *arXiv preprint arXiv:2408.12616*, 2024.
- [56] P. Jiang, C.-K. Wen, X. Li, S. Jin, and G. Y. Li, "Semantic satellite communications based on generative foundation model," *IEEE J. Select. Areas Commun.*, (Early Access), Apr. 2025.
- [57] L. Qiao, M. B. Mashhadi, Z. Gao, C. H. Foh, P. Xiao, and M. Bennis, "Latency-aware generative semantic communications with pre-trained diffusion models," *IEEE Wireless Commun. Lett.*, vol. 13, no. 10, pp. 2652–2656, Oct. 2024.
- [58] Y. Wang, S. Han, X. Xu, H. Liang, R. Meng, C. Dong, and P. Zhang, "Feature importance-aware task-oriented semantic transmission and optimization," *IEEE Trans. Cogn. Commun. Netw.*, vol. 10, no. 4, pp. 1175–1189, Aug. 2024.
- [59] G. Zhang, Q. Hu, Y. Cai, and G. Yu, "SCAN: Semantic communication with adaptive channel feedback," *IEEE Trans. Cogn. Commun. Netw.*, vol. 10, no. 5, pp. 1759–1773, Oct. 2024.
- [60] Z. Weng, Z. Qin, H. Xie, X. Tao, and K. B. Letaief, "Semantic MIMO systems for speech-to-text transmission," *IEEE Trans. Wireless Commun.*, vol. 23, no. 12, pp. 18697–18710, Dec. 2024.
- [61] S. Guo, Y. Wang, S. Li, and N. Saeed, "Semantic importance-aware communications using pre-trained language models," *IEEE Commun. Lett.*, vol. 27, no. 9, pp. 2328–2332, Sep. 2023.

- [62] P. Jiang, C.-K. Wen, S. Jin, and G. Y. Li, "Deep source-channel coding for sentence semantic transmission with HARQ," *IEEE Trans. Commun.*, vol. 70, no. 8, pp. 5225–5240, Aug. 2022.
- [63] Z. Xiao, S. Yao, J. Dai, S. Wang, K. Niu, and P. Zhang, "Wireless deep speech semantic transmission," in *Proc. IEEE Int. Conf. Acoust., Speech, Signal Process. (ICASSP)*, Rhodes Island, Greece, Jun. 2023, pp. 1–5.
- [64] P. Jiang, C.-K. Wen, S. Jin, and G. Y. Li, "RIS-enhanced semantic communications adaptive to user requirements," *IEEE Trans. Commun.*, vol. 72, no. 7, pp. 4134–4148, Jul. 2024.
- [65] P. Series, *Propagation Data and Prediction Methods Required for the Design of Earth-Space Telecommunication Systems*, ITU, Geneva, Switzerland, Rec. ITU-R P. 618-12, 2015.
- [66] O. Kondrateva, S. Dietzel, and B. Scheuermann, "Joint source-and-channel coding for small satellite applications," in *Proc. 2023 IEEE 48th Conf. Local Comput. Netw. (LCN)*, Daytona Beach, FL, USA, Oct. 2023, pp. 1–9.
- [67] J. Booth, A. Roussos, S. Zafeiriou, A. Ponniah, and D. Dunaway, "A 3D morphable model learnt from 10,000 faces," in *Proc. IEEE Conf. Comput. Vis. Pattern Recognit.*, Las Vegas, NV, USA, Jun. 2016, pp. 5543–5552.
- [68] Y. Deng, J. Yang, S. Xu, D. Chen, Y. Jia, and X. Tong, "Accurate 3D face reconstruction with weakly-supervised learning: From single image to image set," in *Proc. IEEE/CVF Conf. Comput. Vis. Pattern Recognit. Workshops*, Long Beach, CA, USA, Jun. 2019, pp. 285–295.
- [69] A. Radford, J. W. Kim, T. Xu, G. Brockman, C. McLeavey, and I. Sutskever, "Robust speech recognition via large-scale weak supervision," in *Proc. 40th Int. Conf. Mach. Learn.*, Honolulu, Hawaii, USA, Jul. 2023, pp. 28 492–28 518.
- [70] M. McAuliffe, M. Socolof, S. Mihuc, M. Wagner, and M. Sonderegger, "Montreal Forced Aligner: Trainable text-speech alignment using Kaldi," in *Proc. Annu. Conf. Int. Speech Commun. Assoc.*, Stockholm, Sweden, Aug. 2017, pp. 498–502.
- [71] Y. Ren, C. Hu, X. Tan, T. Qin, S. Zhao, Z. Zhao, and T.-Y. Liu, "Fastspeech 2: Fast and high-quality end-to-end text to speech," in *Proc. 9th Int. Conf. Learn. Represent. (ICLR)*, Vienna, Austria, May 2021, pp. 1–15.
- [72] J. Kong, J. Kim, and J. Bae, "HiFi-GAN: Generative adversarial networks for efficient and high fidelity speech synthesis," in *Proc. Adv. Neural Inf. Process. Syst. (NeurIPS)*, vol. 33, Virtual, Dec. 2020, pp. 17 022–17 033.
- [73] Z. Ye, T. Zhong, Y. Ren, J. Yang, W. Li, J. Huang, Z. Jiang, J. He, R. Huang, J. Liu *et al.*, "Real3d-portrait: One-shot realistic 3d talking portrait synthesis," *arXiv preprint arXiv:2401.08503*, 2024.
- [74] B. Martinez, P. Ma, S. Petridis, and M. Pantic, "Lipreading using temporal convolutional networks," in *Proc. IEEE Int. Conf. Acoust., Speech, Signal Process. (ICASSP)*, Barcelona, Spain, Barcelona, Spain, May 2020, pp. 6319–6323.
- [75] G. Cong, L. Li, Y. Qi, Z.-J. Zha, Q. Wu, W. Wang, B. Jiang, M.-H. Yang, and Q. Huang, "Learning to dub movies via hierarchical prosody models," in *Proc. IEEE/CVF Conf. Comput. Vis. Pattern Recognit. (CVPR)*, Vancouver, Canada, Jun. 2023, pp. 14 687–14 697.
- [76] J. Deng, J. Guo, N. Xue, and S. Zafeiriou, "ArcFace: Additive angular margin loss for deep face recognition," in *Proc. IEEE/CVF Conf. Comput. Vis. Pattern Recognit. (CVPR)*, Long Beach, CA, USA, Jun. 2019, pp. 4690–4699.
- [77] T. Afouras, J. S. Chung, A. Senior, O. Vinyals, and A. Zisserman, "Deep audio-visual speech recognition," *IEEE Trans. Pattern Anal. Mach. Intell.*, vol. 44, no. 12, pp. 8717–8727, Dec. 2022.
- [78] A. Nagrani, J. S. Chung, and A. Zisserman, "Voxceleb: a large-scale speaker identification dataset," *arXiv preprint arXiv:1706.08612*, 2017.
- [79] Z. Weng and Z. Qin, "Semantic communication systems for speech transmission," *IEEE J. Sel. Areas Commun.*, vol. 39, no. 8, pp. 2434–2444, Aug. 2021.
- [80] R. Zhang, P. Isola, A. A. Efros, E. Shechtman, and O. Wang, "The unreasonable effectiveness of deep features as a perceptual metric," in *Proc. IEEE/CVF Conf. Comput. Vis. Pattern Recognit. (CVPR)*, Utah, USA, Jun. 2018.
- [81] A. Siarohin, S. Lathuilière, S. Tulyakov, E. Ricci, and N. Sebe, "First order motion model for image animation," in *Proc. Adv. Neural Inf. Process. Syst. (NeurIPS)*, Vancouver, Canada, Dec. 2019, pp. 7137–7147.
- [82] A. W. Rix, J. G. Beerends, M. P. Hollier, and A. P. Hekstra, "Perceptual evaluation of speech quality (PESQ)-a new method for speech quality assessment of telephone networks and codecs," in *Proc. IEEE Int. Conf. Acoust., Speech Signal Process. (ICASSP)*, Salt Lake City, UT, USA, May 2001, pp. 749–752.
- [83] K. R. Prajwal, R. Mukhopadhyay, V. P. Nambodiri, and C. V. Jawahar, "A lip sync expert is all you need for speech to lip generation in the wild," in *Proc. 28th ACM Int. Conf. Multimedia (ACM MM)*, Seattle, WA, USA, Oct. 2020, pp. 484–492.